STUDY AND CHARACTERIZATION OF MONOLITHIC

ACTIVE PIXEL SENSORS (MAPS) FOR HIGH

ENERGY PARTICLE DETECTORS

Natthawut Laojamnongwong

A Thesis Submitted in Partial Fulfillment of the Requirements for the

Degree of Master of Science in Applied Physics

Suranaree University of Technology

Academic Year 2018

การศึกษาและวิเคราะห์คุณลักษณะเบื้องต้นของ Monolithic Active Pixel Sensors (MAPS) สำหรับเครื่องตรวจจับอนุภาคพลังงานสูง

นายณัฐวุฒิ เหล่าจำนงค์วงษ์

วิทยานิพนธ์นี้เป็นส่วนหนึ่งของการศึกษาตามหลักสูตรปริญญาวิทยาศาสตรมหาบัณฑิต

สาขาวิชาฟิสิกส์ประยุกต์

มหาวิทยาลัยเทคโนโลยีสุรนารี

ปีการศึกษา 2561

STUDY AND CHARACTERIZATION OF MONOLITHIC ACTIVE PIXEL SENSORS (MAPS) FOR HIGH ENERGY PARTICLE DETECTORS

Suranaree University of Technology has approved this thesis submitted in partial fulfillment of the requirements for a Master's Degree.

Thesis Examining Committee

_____

(Asst. Prof. Dr. Panomsak   Meemon)

Chairperson

_____

(Asst. Prof. Dr. Chinorat   Kobdaj)

Member (Thesis Advisor)

_____

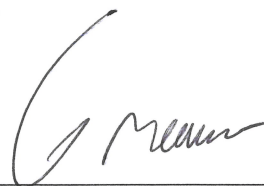(Dr. Kritsada   Kittimanapun)

Member

_____

(Dr. Narong   Chanlek)

Member

_____

(Asst. Prof. Dr. Ayut   Limphirat)

Member

_____

(Prof. Dr. Santi   Maensiri)

Vice Rector for Academic Affairs

and Internationalization

_____

(Assoc. Prof. Dr. Worawat   Meevasana)

Dean of Institute of Science

ฉัฐวุฒิ เหล่าจำนงค์วงษ์ : การศึกษาและวิเคราะห์คุณลักษณะเบื้องต้นของ Monolithic Active Pixel Sensors (MAPS) สำหรับเครื่องตรวจจับอนุภาคพลังงานสูง (STUDY AND CHARACTERIZATION OF MONOLITHIC ACTIVE PIXEL SENSORS (MAPS) FOR HIGH ENERGY PARTICLE DETECTORS) อาจารย์ที่ปรึกษา : ผู้ช่วยศาสตราจารย์ ดร.ชิโนรัตน์ กอบเดช, 77 หน้า.

Monolithic Active Pixel Sensors (MAPS) เป็นเซนเซอร์รับภาพ (image sensor) ถูกสร้างขึ้นด้วยชิป (chip) ที่รวมระบบเซนเซอร์และการอ่านสัญญาณ (read-out) เข้าด้วยกัน MAPS ถูกเสนอให้นำมาใช้เป็นเซนเซอร์สำหรับตรวจจับอนุภาคพลังงานสูงที่ห้องปฏิบัติการไอออนหนักอลิซ (ALICE) มหาวิทยาลัยเทคโนโลยีสุรนารีและสถาบันวิจัยแสงซินโครตรอนในฐานะสมาชิกของ ALICE ร่วมมือกันทำงานร่วมกับทีม ALICE ในการวิจัยและพัฒนาเซนเซอร์ชนิดนี้ MAPS มีการออกแบบและพัฒนาต้นแบบต่าง ๆ เช่น Explorer และ ALPIDE ในงานนี้ ALPIDE ได้ถูกนำมาทดสอบประสิทธิภาพในการตรวจจับอนุภาคโดยการใช้ลำอิเล็กตรอนพลังงาน 1 GeV ที่มีการปรับความเข้มของลำอนุภาคให้มีค่าประมาณ 10 electrons/bunch ณ สถานีทดลองลำอิเล็กตรอนของสถาบันวิจัยแสงซินโครตรอน (SLRI Beam Test Facility)

จากการทดสอบพบว่าประสิทธิภาพในการตรวจจับอนุภาคของ ALPIDE เซนเซอร์มีประสิทธิภาพถึงร้อยละ 99.6 ซึ่งการทดสอบดังกล่าวแสดงให้เห็นว่า ALIPDE เซนเซอร์มีประสิทธิภาพพอที่จะนำไปติดตั้งในหัววัดการติดตามเส้นทางเดินของอนุภาค (Inner Tracking System) ของเครื่องตรวจจับอนุภาค ALICE ระหว่างการปิดปรับปรุงเครื่องชนอนุภาคฮาดรอนขนาดใหญ่ (Large Hadron Collider; LHC) ในปี 2019 – 2020

สาขาวิชาฟิสิกส์   ลายมือชื่อนักศึกษา_____

ปีการศึกษา 2561   ลายมือชื่ออาจารย์ที่ปรึกษา_____

ลายมือชื่ออาจารย์ที่ปรึกษาร่วม_____

ลายมือชื่ออาจารย์ที่ปรึกษาร่วม_____

NATTHAWUT LAOJAMNONGWONG : STUDY AND
CHARACTERIZATION OF MONOLITHIC ACTIVE PIXEL SENSORS
(MAPS) FOR HIGH ENERGY PARTICLE DETECTORS. THESIS
ADVISOR : ASST. PROF. CHINORAT KOBDAJ, Ph.D. 77 PP.

ALICE/PARTICLE DETECTOR/MONOLITHIC ACTIVE PIXEL SENSORS

Monolithic Active Pixel Sensors (MAPS) are image sensors built with the on-chip integration of sensors and a signal readout system. MAPS have recently been proposed as sensors for detection of high energy particles at A Large Ion Collider Experiment (ALICE). Suranaree University of Technology (SUT) and Synchrotron Light Research Institute (SLRI), as members of the ALICE collaboration, have been working together with the ALICE team on research and development of these sensors. Several MAPS prototypes such as Explorer and pALPIDE have been designed and developed. In this work, ALPIDE was tested for the detection efficiency with 1 GeV electron beam. The intensity of electron beam was approximately 10 electron/bunch at SLRI Beam Test Facility.

Based on our test results, the detection efficiency of the ALPIDE sensor is 99.6%. The results showed that the ALPIDE sensor had sufficiently good performance to be installed in the Inner Tracking System of the ALICE detector during the shutdown of the Large Hadron Collider (LHC) in 2019 - 2020.
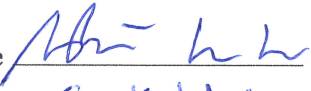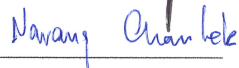
School of Physics

Academic Year 2018

Student's Signature

Advisor's Signature _C. Kobdaj_

Co-advisor's Signature

Co-advisor's Signature _Nawang Chanlek_

ACKNOWLEDGEMENTS

CONTENTS

CONTENTS (Continued)

CONTENTS (Continued)

LIST OF TABLES

LIST OF FIGURES

LIST OF FIGURES (Continued)

LIST OF FIGURES (Continued)

LIST OF FIGURES (Continued)

LIST OF FIGURES (Continued)

LIST OF ABBREVIATIONS

ALICE   A Large Ion Collider Experimental

ITS   Inner Tracking System

QGP   Quark-Gluon Plasma

TPC   Time Projection Chamber

TOF   Time-Of-Flight

MAPS   Monolithic Active Pixel Sensor

PID   Particle Identification

SPD   Silicon Pixel Detectors

SDD   Silicon Drift Detectors

SSD   Silicon Strip Detectors

PHOS   Photon Spectrometer

EMCal   Electromagnetic Calorimeter

HMPID   High Momentum Particle Identification

RICH   Ring Imaging Cherenkov

HFT   Heavy Flavor Tracker

ASIC   Application Specific Integrated Circuits

STAR   Solenoidal Tracker

RHIC   Relativistic Heavy Ion Collider

SLRI   Synchrotron Light Research Institute

BTF   Beam Test Facility

LIST OF ABBREVIATIONS (Continued)

HBT	High-energy Beam Transport line
LBT	Low-energy Beam Transport line
QF	Quadrupole Focusing
QD	Quadrupole Defocuing
BH	Bending Magnet Horizontal
BV	Bending Magnet Vertical
DUT	Device Under Test
MIPs	Minimum Ionizing particles
DAQ	Data acquisition
FIFO	First-In First-Out
DAC	Digital to Analog Converter
SRAM	Static Random-Access Memory

CHAPTER I

INTRODUCTION

A Large Ion Collider Experiment (ALICE) is one of the most important experiments of the Large Hadron Collider (LHC) at the European Organization for Nuclear Research (CERN). It is a complex high-energy particle detector system that is optimized to study heavy-ion (Pb-Pb nuclei) collisions at a center of mass energy of 5.5 TeV per nucleon pair, in particular, the properties of the Quark-Gluon Plasma (QGP), the state of a particle at extremely high temperature and density. This state is expected to exist a few milliseconds after the Big Bang. ALICE has planned to upgrade the Inner Tracking System (ITS) in order to improve the measurement precision and increase of event readout rate. ALICE has been preparing to install the new ITS during the second long shutdown (LS2) of LHC in 2019 - 2020. (Satz, 2011; Aamodt et al., 2008; ALICE collaboration, 2012; ALICE Collaboration, 2014).

1.1 The ALICE detector

The schematic diagram of the ALICE detector is shown in Figure 1.1. The ALICE detector that is 26-m long and 16-m high consists of several sub-detector systems. These detectors are mainly dedicated for vertex reconstruction, tracking, and particle identification (PID).

- The Time Projection Chamber (TPC) is a detector for tracking and particle identification via specific energy loss. It is a gaseous detector in the shape of a hollow cylinder with length of 5m in beam direction. An inner radius

is approximately 57 cm and an outer radius is 278 cm, comprising an active gas volume of 88 m^3.

- The Time-Of-Flight (TOF) consists of multi-gap resistive plate chambers (RPC) at a radial distance of 370 cm from the beam line. It is designed for PID by measuring the flight time from the interaction point.

- The most important detector is an Inner Tracking System (ITS). It is used to locate the primary vertex and reconstruct the secondary vertex. The ITS consists of six cylindrical layers of position sensitive silicon detectors, covering radial distance between 39mm and 436mm. It is built using three different technologies: hybrid Silicon Pixel Detectors (SPD) for the two inner layers, Silicon Drift Detectors (SDD) for the two middle layers and Silicon Strip Detectors (SSD) for the two outer layers. The main purpose is the precise determination of primary and secondary vertices with high granularity, at low transverse momentum $p_\perp$ tracking.

- Photon Spectrometer (PHOS) is a high resolution electromagnetic calorimeter consisting of 17,920 detection channels based on leadtungstate crystals (PbWO4).

- ElectroMagnetic Calorimeter (EMCal) is designed to provide the following functions: efficient and unbiased fast level L0 and L1 trigger on high energy jets; measurement of the neutral portion of jet energy; improvement of jet energy resolution; measurement of high momentum photons, π^0 and electrons; γ/π^0 discrimination up to 30 GeV (considering invariant mass and shower shape techniques only); electron/hadron separation for momenta larger than 10 GeV/c; high uniformity of response for isolated electromagnetic clusters.

- The High Momentum Particle Identification (HMPID) is based on proximity focusing Ring Imaging Cherenkov (RICH) counters and consists of seven modules mounted in an independent support cradle, which will be fixed to the space frame, at two o'clock position.
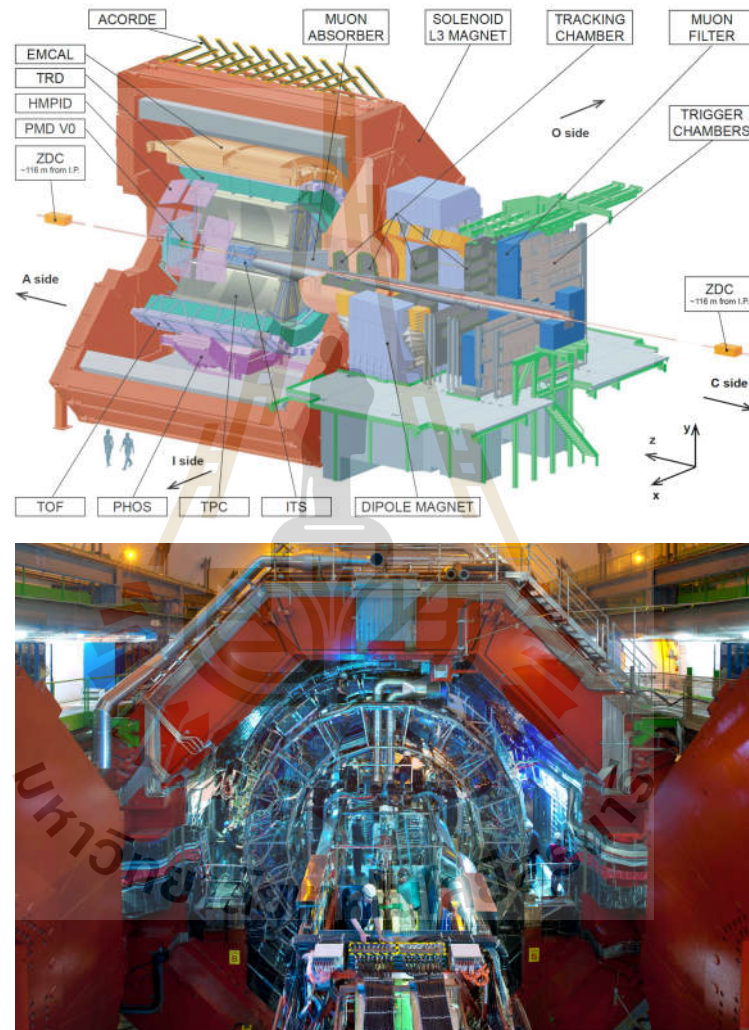
Figure 1.1 Schematic diagram (top) and photograph (bottom) of the ALICE experiment (Aamodt et al., 2008).

1.2 Inner Tracking System (ITS)

The main tasks of the Inner Tracking System are to reconstruct the primary and secondary vertexes, to track and identify changed particles with a low transverse momentum, and to improve momentum resolution at the high transverse momentum.

The present ALICE ITS consists of six cylindrical layers of silicon detectors placed coaxially around the beam pipe. Its layout is shown in Figure 1.2. The two innermost layers are made of Silicon Pixel Detectors (SPD), the two central layers are made of Silicon Drift Detectors (SDD) and the two outermost layers of double sided Silicon Strip Detectors (SSD). The silicon detectors will be changed to Monolithic Active Pixel Sensors (MAPS) for improvement of sensor's performance (Yang et al., 2015).

Table 1.1 Dimensions of the current ITS detectors (active areas).

Layer	Type	r (cm)	$\pm z$(cm)	Area (m^2)
1	pixel	3.9	14.1	0.07
2	pixle	7.6	14.1	0.14
3	drift	15	22.2	0.42
4	drift	23.9	29.7	0.89
5	strip	38	43.1	2.20
6	strip	43	48.9	2.80
Total area				6.28
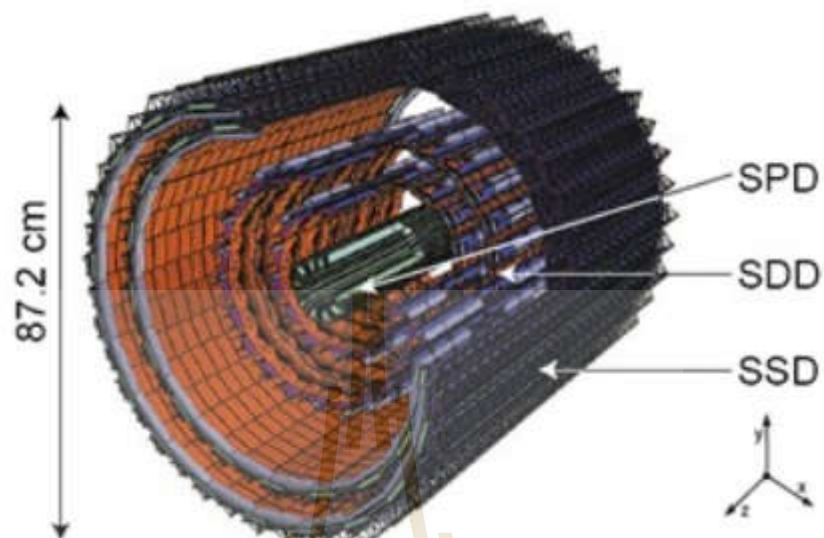
Figure 1.2 Layout of the present ALICE ITS (ALICE collaboration, 2010).
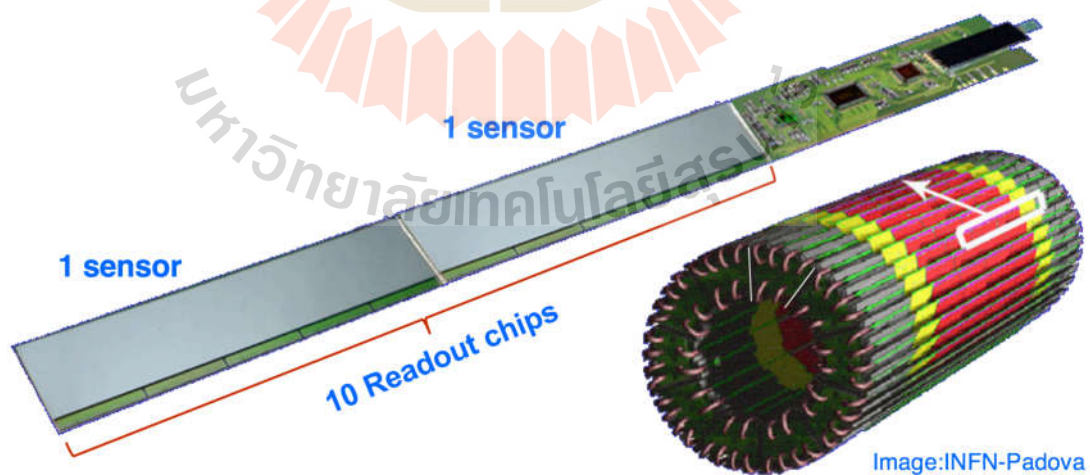
Figure 1.3 Layout of the Silicon Pixel Detectors (SPD) innermost layers of present ALICE ITS.

1.3 ALICE ITS upgrade plans

ALICE has planned to upgrade the Inner Tracking System (ITS) during the second-long shutdown of the LHC in 2019-2020. The ITS upgrade concepts are to improve the measurement of the impact parameter resolution by reducing the beam pipe diameter in the center of the ALICE detector and minimizing material budget of the detector structure. As a result, the tracking performance and momentum resolution are expected to be improved. The use of MAPS will grant the silicon material budget per layer to be reduced from 350 μm of the present ITS to 50 μm of the upgrade ITS. An example of the feasibility of such design is shown by the STAR Heavy Flavor Tracker (HFT) detector (Dorokhov et al., 2011).

The ITS upgrade detailed simulations have been performed to determine the optimum design parameters. In summary, the following design objectives were defined:

- Reducing the distance between the first layer and the interaction point from 39 mm to 22 mm

- Reducing the material budget from 1.14 % to 0.3 % x/X_0 per layer for the innermost layers and to 1.0 % x/X_0 per layer for the outer layers

- Reducing the pixel size from 50 μm $\times$ 425 μm to about 30 μm $\times$ 30 μm

- Increasing the number of layers from currently six to seven; this will also improve the standalone tracking efficiency and $p_\perp$-resolution at low transverse momenta.

- Increasing the readout rate from currently maximum 1 kHz to up to 100 kHz for Pb-Pb collisions and 400 kHz for pp collisions

- Implementation of the possibility for an efficient insertion and removal of detector parts during the yearly shutdown period

The new ITS consists of seven cylindrical layers of silicon detectors placed coaxially around the beam pipe. A layout is included as shown in Figure 1.4 (ALICE Collaboration, 2014). The seven layers are divided into two separate barrels (inner barrel and outer barrel), each of which has different specifications, as shown in Figure 1.5. The inner barrel consists of the three layers, also referred to as Inner Layers, while the outer barrel contains the four layers, also referred as outer layers.
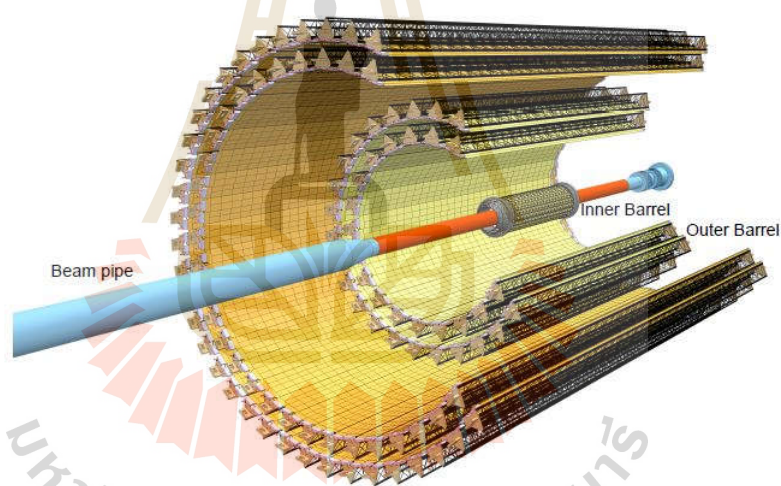
Figure 1.4 Layout of the new ALICE ITS (ALICE Collaboration, 2014).
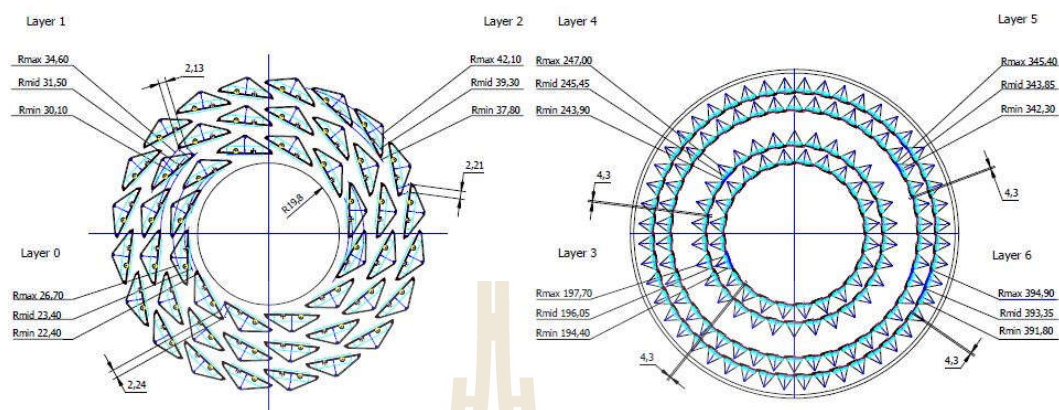
Figure 1.5 Schematic view of the cross section of the Inner Barrel (left) and Outer Barrel (right) (ALICE Collaboration, 2014).
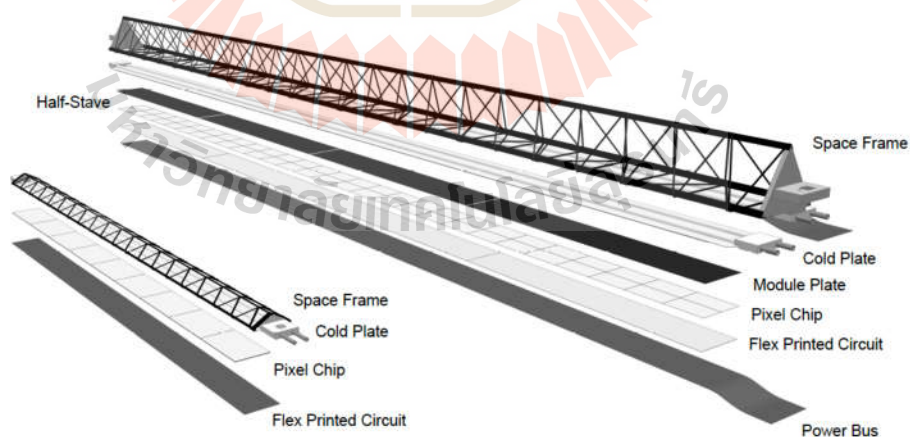
Figure 1.6 Schematic drawing of the Inner Barrel (left) and Outer Barrel (right) staves (ALICE Collaboration, 2014).

Particle sensors and the associated read-out electronics, used for vertexing and tracking detection systems, must be qualified in terms of granularity, material thickness, read-out speed, power consumption and radiation hardness. The ITS sensor and its read-out electronic are developed based on silicon (Si) semiconductor technology and CMOS technology respectively. These technologies can be optimized by thinning both sensor and read-out Application Specific Integrated Circuits (ASIC) as well as reducing the bump-bonding pitch as much as possible. Nevertheless, there are some technical limitations of the present detectors. In order to go beyond these limitations, ALICE has developed the ITS with new technology. The optimal way to achieve is to integrate both sensor and read-out electronics to create a single detection device. This approach is taken by CMOS Monolithic Active Pixels Sensors (MAPS) (Kofarago, 2015).

1.4   Research objective

This thesis is the preliminary characterization of the ALPIDE sensor both with the test system in the laboratory and the 1 GeV electron beam at the Synchrotron Light Research Institute Beam Test Facility (SLRI-BTF). The upgrade of ITS, including its motivation and the requirements on the Monolithic Active Pixel Sensors derived, are discussed in detailed in the chapter II. The detailed commissioning of the SLRI-BTF is given in the next chapter III. Chapter IV presents detailed of the pixel Telescope setup at SLRI-BTF. The first test beam results and preliminary characterization on the final ALPIDE were discussed in chapter V. The final chapter VI is the conclusion of this thesis.

1.5 ALICE ITS physics motivation

The main physics motivation for the upgrade of the Inner Tracking System of the ALICE experiment is to perform new measurements on heavy flavour (charm and beauty) and thermal dilepton production in heavy-ion collisions. The goals are to address important questions about the QGP properties that cannot be answered with the present experimental setup (ALICE Collaboration, 2014).

- The study of the thermalization and hadronization of heavy quarks in the QGP medium. This will be possible by measuring the heavy flavour baryon/meson ratio for charm (Λ_c/D) and for beauty (Λ_b/D), and the azimuthal anisotropy v_2 for charm and beauty mesons.

- The study of the in-medium energy loss of heavy quarks and its mass dependence. This can be performed by measuring the nuclear modification factors R_{AA} as function of $p_\perp$ for D and B mesons in a wide momentum range, as well as the heavy flavour production associated with jets.

Table 1.2 Summary of physics ability in term of the minimum accessible transverse momentum p_T and of statistical uncertainties for an integrated luminosity 10 nb^{-1} with minimum-bias data collection. (ALICE Collaboration, 2014).

Observable	Current, 0.1 nb^{-1}		Upgrade, 10 nb^{-1}	
	p_T^{Amin} (GeV/c)	statistical uncertainty	p_T^{Amin} (GeV/c)	statistical uncertainty
Heavy Flavour				
D meson R$_{\mathrm{AA}}$	1	10%	0	0.3%
D$_s$ meson R$_{\mathrm{AA}}$	4	15%	< 2	3%
J/ψ from B R$_{\mathrm{AA}}$	1.5	15%	1	5%
B$^+$ yield	not accessible		2	10%
Λ_c R$_{\mathrm{AA}}$	not accessible		2	15%
Λ_c/D^0 ratio	not accessible		2	15%
Λ_b yield	not accessible		7	20%
D$_s$ meson v_2 ($v_2 = 0.2$)	not accessible		< 2	8%
D from B v_2 ($v_2 = 0.05$)	not accessible		2	8%
J/ψ from B v_2 ($v_2 = 0.05$)	not accessible		1	60%
Λ_c v_2 ($v_2 = 0.15$)	not accessible		3	20%
Di-electrons				
Temperature (intermediate mass)	not accessible			10%
Elliptic flow ($v_2 = 0.1$)	not accessible			10%
Low-mass spectral function	not accessible		0.3	20%
Hypernuclei				
$^3_\Lambda$H yield	2	18%	2	1.7%

CHAPTER II

MONOLITHIC ACTIVE PIXEL SENSORS

Monolithic Active Pixel Sensors (MAPS) are image sensors that both read-out electronics and sensors are integrated on the same piece of the silicon substrate. It was first introduced for high-energy particle experiments in the upgrade of the inner detector of the Solenoidal Tracker (STAR) at the Relativistic Heavy Ion Collider (RHIC) to improve the vertex resolution (Dorokhov et al., 2011; Schambach et al., 2015; Kittimanapun et al., 2017). During the research and development procedure, it has gone through the stringent tests under both radiation sources and high-energy particle beams to meet all desired specifications. Finally, the ULTIMATE sensor which is the first MAPS has been implemented successfully in STAR (Mager, 2016).

2.1 Charge Generation in Silicon

The principle of solid state detectors is based on the energy loss of traversing particles or radiation in the sensor material. Part of the energy is lost to the generation of free electron-hole $(e - h)$ pairs, which induce a signal current on their respective collection electrodes.

For silicon, the mean energy w required to create a single $e-h$ pair is about 3.6 eV, which is three times larger than the band gap (1.12 eV). The difference goes to the generation of phonons and the dissipation of thermal energy.

Due to the varying fractions of deposited energy used for charge carrier and phonon generation, the variance of the number of $e - h$ pairs N_{e-h} generated by

a deposited energy E is reduced by the Fano factor F according to

$$\langle \Delta N_{\text{e-h}}^2 \rangle = F N_{\text{e-h}} = F \frac{E}{w} \tag{2.1}$$

For most semiconductors being in the order of 0.1, the Fano factor determines the best possible energy resolution of semiconductor sensors.

2.1.1 Energy loss of charged particles

Charged particles crossing material deposit part of their energy by means of scattering processes with the electrons in medium, causing approximately uniform ionization along the path. For particles heavier than electrons, this process is described by the Bethe-Bloch formula (Nakamura, 2010),

$$-\frac{1}{\rho} \left\langle \frac{dE}{dx} \right\rangle = 4\pi N_A r_e^2 m_e c^2 z^2 \frac{Z}{A} \frac{1}{\beta^2} \left(\frac{1}{2} \ln \left(\frac{2 m_e c^2 \beta^2 \gamma^2 T_{max}}{I^2} \right) - \beta^2 \right) \tag{2.2}$$

with:

N_A: Avogrado's number;

z: charge of the traversing particle in terms of unit charge;

Z: atomic number of the absorption medium (14 for silicon);

A: atomic mass of the absorption medium (28 g/mol for silicon);

$m_e c^2$: rest energy of the electron;

r_e: classical electron radius;

β: velocity of the traversing particle in units of c;

γ: Lorentz factor $1/\sqrt{1 - \beta^2}$;

I: mean excitation energy (137 eV for silicon);

$T_{max} = \frac{2m_e c^2 \beta^2 \gamma^2}{1 + 2\gamma m_e/M + (m_e/M)^2}$: maximum energy loss for a particle with mass M in a single collision;

Equation 2.2 represents the average differential energy loss per mass surface density, typically expressed in $\left[\frac{MeV}{g/cm^2}\right]$. There exist additional correction term to equation 2.2 as the density correction for high energy particles and the shell correction for low energy ones. For electrons and positrons, additional modifications to the Bethe-Bloch formula are required due to their low mass and the fact that they interact with identical particles (i.e., electrons) while traversing the medium. Furthermore, additional energy-loss mechanisms such as bremsstrahlung have to be considered.

2.2 Pixel detector

The pixel detector is the image processing device. It has been developed for particle physics application, and development for imaging applications in biomedicine and astronomy. In this section, we will talk about the pixel detector for high-energy particle detectors, which is a hybrid pixel sensor and a monolithic active pixel sensor. Both sensors are applied for the vertexing and tracking in the innermost region of ALICE ITS. The hybrid pixel detector consists of the sensors and electronic readout device, which are connected to each other by using fine pitch bump-bonding. The monolithic active pixel sensor is the sensor that the readout electronics are integrated on the same silicon wafer, completely avoiding bum-bonding for reducing the material budget.

The hybrid pixel sensor is the sensor that a readout chip is a separate component. Each charge collection diode (pixel cell) in the sensor is connected via

micro-bump bonds to the corresponding cell in the readout chip. The deep p-well is a feature of the TowerJazz 180 μm CMOS process. The schematic cross sections through pixel sensors is shown in Figure 2.1.
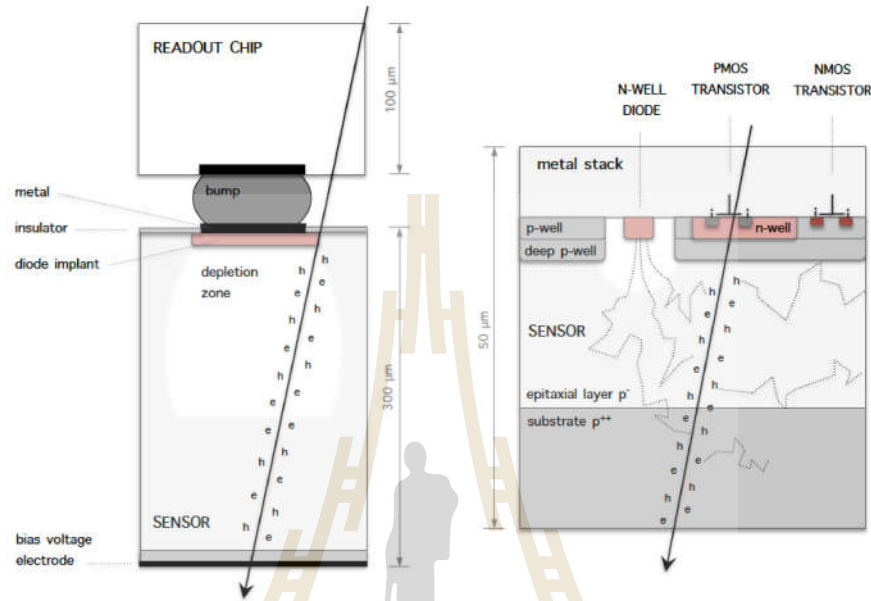
Figure 2.1 Schematic cross sections of sensors with different technologies, hybrid pixel sensor (left) and monolithic pixel sensor (right).

2.3   Semiconductor

2.3.1   Silicon Properties

In silicon, electron-hole $(e-h)$ pairs are constantly being thermally excited. Under stable conditions, an equilibrium between the two process is established and the $e-h$ pair concentration n_i is proportional to $T^{3/2}exp(-E_g/2kT)$. Energy gap of 3.6 eV is required to excite an electron from valence to conduction band, k is the Boltzmann constant, and T is the absolute temperature. At room temperature $n_i \cong 2.5 \times 10^{13} \text{cm}^{-3}$. The resistivity of a semiconductor is given by, where e is the elementary charge and μ_e and μ_h are electron and hole mobilities. Their values

in silicon are 1350 and 480 $cm^2V^{-1}s^{-1}$. Therefore intrinsic silicon at 300 K has resistivity $\rho = 230$ kΩcm.

$$\rho = \frac{1}{en_i(\mu_e + \mu_h)} \tag{2.3}$$

2.3.2 Junctions

Adding pentavalent atoms to the silicon crystal, an n-type silicon is obtained, while adding trivalent atoms results in a p-type silicon. This process is called doping, and the pentavalent and trivalent atoms are called donors and acceptors. Both processes introduce additional energy levels in the silicon band structure.
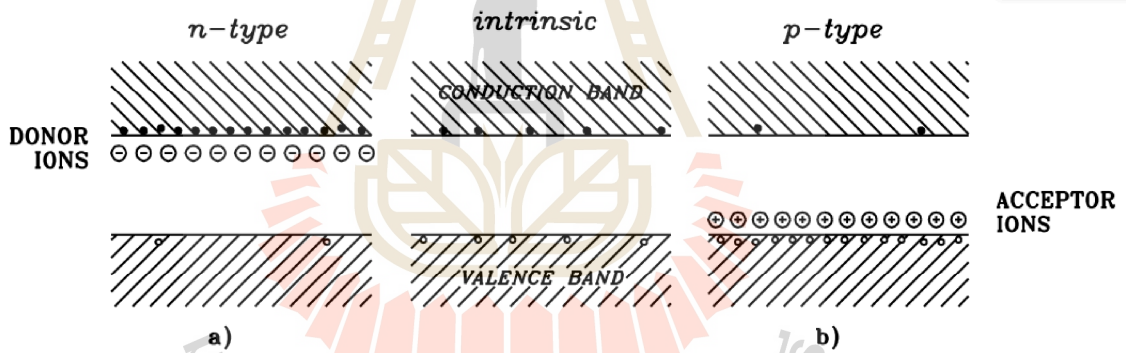
Figure 2.2 Silicon band structure - Schematic energy band representation of extrinsic n-type (a) and p-type (b) semi-conductors.

2.3.3 Anisotype Junction ($p - n$)

The concentration difference of electrons and holes in the two different regions causes diffusion of electrons towards p-type silicon and holes toward n-type silicon. Electrons fill-up holes and holes capture electrons, creating a potential difference (built-in potential) between the two initially neutral regions (p-type

becomes negative while n-type becomes positive). When equilibrium is established, the contact region is devoid of charge carriers and therefore is called the depleted region. Any charge carrier entering or created in this region is accelerated by the electric field (electrons towards n-type and holes towards p-type).
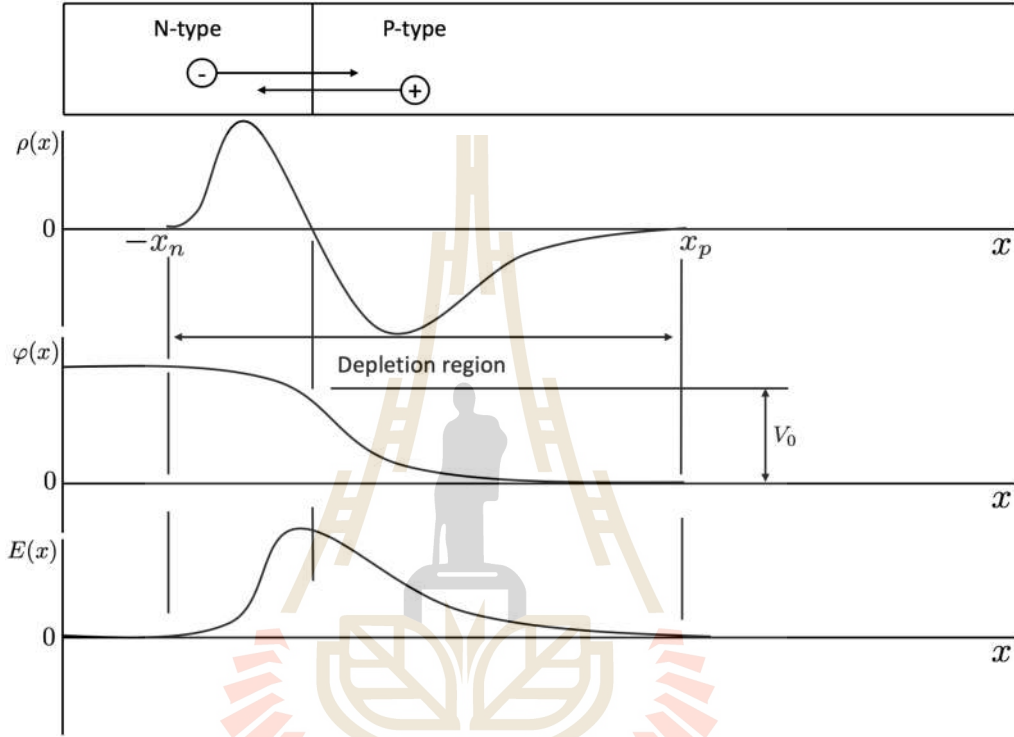
Figure 2.3 P-N junction: The effect of carrier diffusion across the junction gives rise to the illustrated profiles for space charge $\rho(x)$, electric potential $\varphi(x)$ and electric field E(x).

2.3.4 Isotype Junction ($n - n^+$ or $p - p^+$)

Isotype junctions can be treated in a similar way. If we take for instance $n - n^+$ junctions, we can consider n and n^+ types in isotype junctions as p and n type in anisotype junctions, respectively. This treatment is not entirely correct since there are no intermediate band levels corresponding to the acceptor atoms. Nevertheless, charge carriers (in this example electrons) diffuse from highly doped

region (n^+) to the region with lower doping level (n). As in $p - n$ junction, two initially neutral regions become charged creating potential difference. Electrons excited in the n-region, in the proximity of the junction, will be attracted toward the n^+ region while holes will be reflected back into the n-region. The situation is opposite in case of the $p - p^+$ junction. Holes are attracted by the p^+ region while electrons are reflected by p^+ region. This is one of the essential properties of silicon (and other semiconductors) exploited in MAPS.

2.4   Reverse bias

One of the applications of the PN-junction is the possibility to apply an external voltage, so called forward bias and reverse bias. In this work we use reverse for measurement the detection efficiency of ALPIDE prototype sensors. The diode sensitive area was depleted by applying the reverse bias voltage to observe the effect of the reverse bias on the charge collection efficiency of sensors. The junction is now reversely biased and the reverse voltage applied is defined as positive bias.

If an external potential is applied across the PN junction such that the positive terminal is connected to the n-type material and the negative terminal is connected to the p-type material, the number of uncovered positive ions in the depletion region of the n-type material will increase due to the large number of "free" electrons drawn to the positive potential of the applied voltage.

For the similar reason, the number of uncovered negative ions will increase in the p-type material. The net effect, therefore, is widening of the depletion region.

The width of the depletion zone, the electric field, and the potential as function of the applied voltage can be calculated by solving the one-dimensional
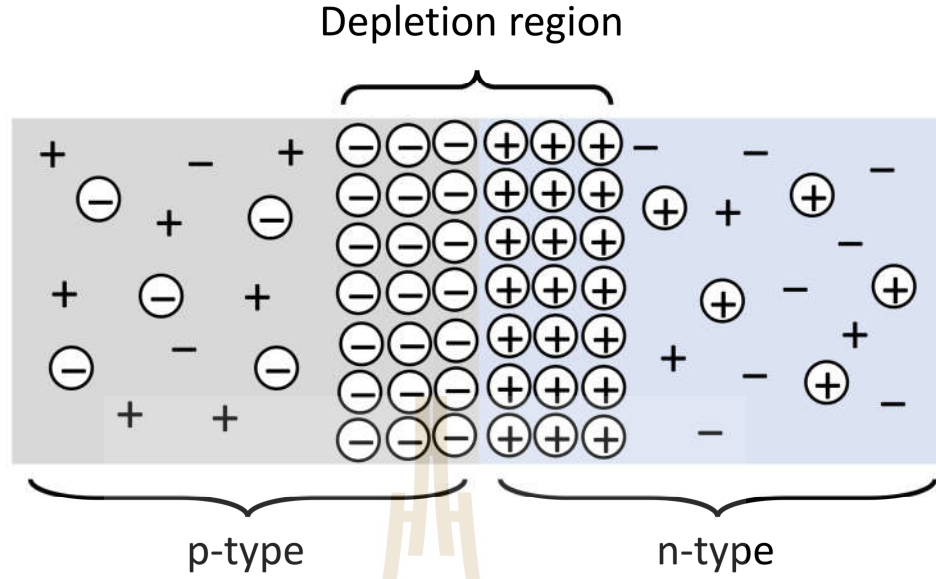
Figure 2.4 Reverse bias PN-junction.

Poisson equation.

$$W = x_n + x_p = \sqrt{\frac{2\varepsilon_0\varepsilon_{Si}}{e}\left(\frac{1}{N_A} + \frac{1}{N_D}\right)(V + V_{bi})} \qquad (2.4)$$

where W is the total width of the depletion zone, x_n is a region of n-type and x_p is a region of p-type, N_D, and N_A are the concentration of donors and acceptors, V_{bi} is bias voltage the space charge region causes an electrical field counteracting the diffusion that can be characterized by the called built-in voltage, and V is the externally applied voltage. In silicon sensors, the junction is usually realized by a shallow and highly doped $p^+ -$ implant in a low-doped bulk material.

2.5 Depletion region

In semiconductor physics, the depletion region refers to the region where the flow of charge carriers of PN-junction, some of the free electrons in the n-type diffuse across the junction and combine with the holes to form p-type near the

(a) $-1\,\mathrm{V}$, $10^{13}\,\mathrm{cm}^{-3}$ (b) $-6\,\mathrm{V}$, $10^{13}\,\mathrm{cm}^{-3}$ (c) $-1\,\mathrm{V}$, $10^{12}\,\mathrm{cm}^{-3}$ (d) $-6\,\mathrm{V}$, $10^{12}\,\mathrm{cm}^{-3}$
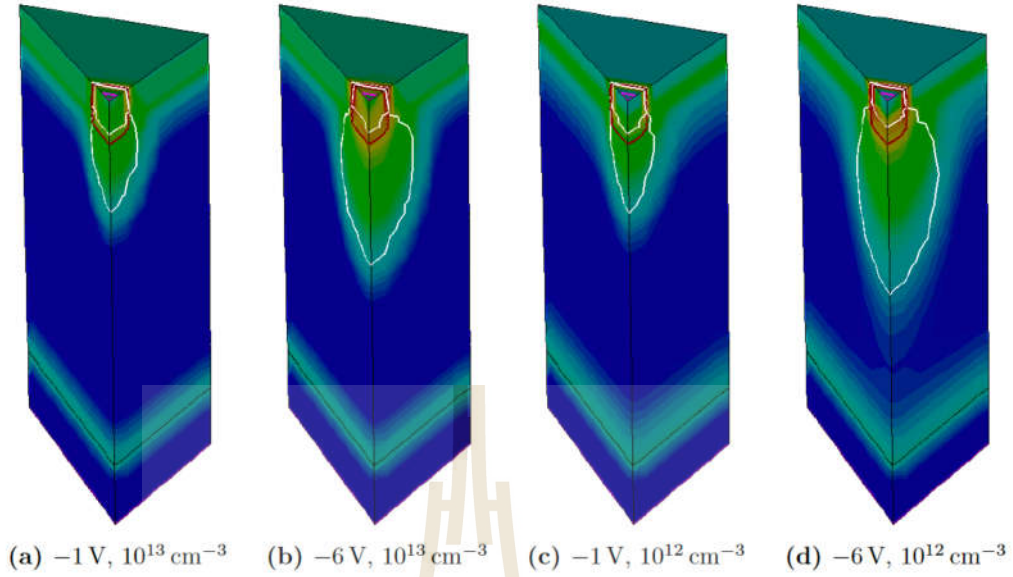
Figure 2.5 Semiconductor device simulations of the different settings of total diode reverse bias and epitaxial layer doping. Shown is one eighth of the total pixel. The colour code shows logarithmically the absolute value of the electrical field, and the white line indicates boundaries of the depletion region. (ALICE Collaboration, 2014).

junction.

When electric potential is applied, small current is produced due to the net migration of the electrons and holes. If the positive terminal is connected to the p-type, this is known as forward bias and results in a smaller depletion zone in Figure 2.8. The opposite, where the positive terminal is connected to the n-type, is known as reverse bias. In this case, the depletion zone is extended. If the reverse bias voltage is great enough, the depletion zone extends all the way to the edge of the semiconductor. This is called full depletion. If the voltage continues to increase, avalanche breakdown will eventually occur.

Without applied voltage, any minority carriers (holes) in the n-type material that find themselves within the depletion region will pass directly into the

p-type material. The closer the minority carrier is to the junction, the higher the attraction for the layer of negative ions and the less the opposite of the positive ions in the depletion region of the *p*-type material. For future discussions we shall assume that all the minority carriers of the *n*-type material that find themselves in the depletion region due to their random motion will pass directly into the *p*-type material. The similar discussion can be applied to the minority carriers (electrons) of the *p*-type material.
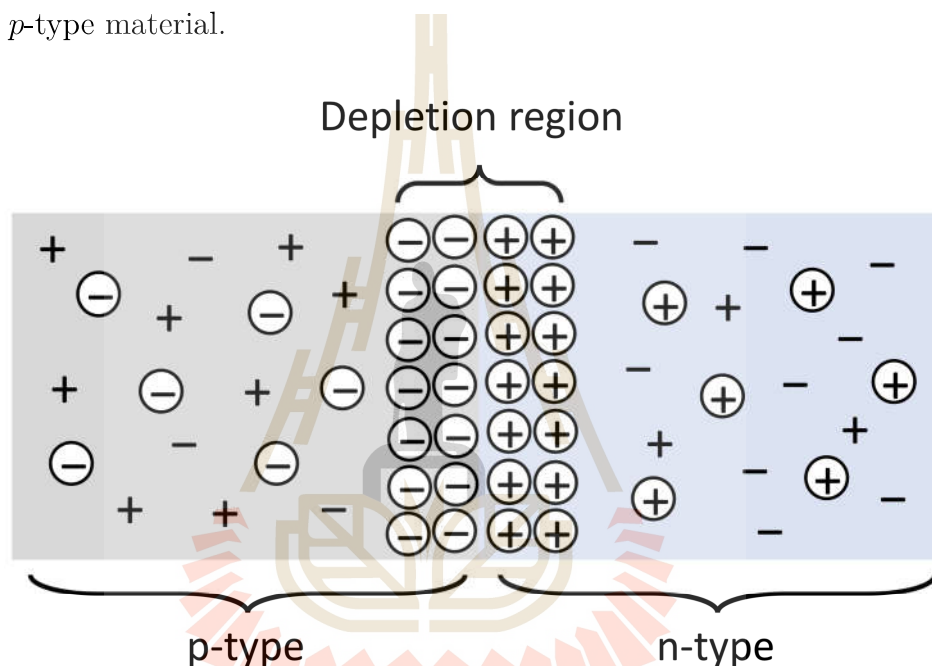
Figure 2.6 PN-junction without applied bias.

Forward-bias is established by applying the positive potential to the *p*-type material and the negative potential to the *n*-type material. The application of a forward-bias will "pressure" electrons in the *n*-type material and holes in the *p*-type material to recombine with the ions near the boundary and reduce the width of the depletion region as shown in Figure 2.8. The resulting minority-carrier flow of electrons from the *p*-type material to the *n*-type material (and of holes from the *n*-type material to the *p*-type material) has not changed in magnitude (since the conduction level is controlled primarily by the limited number of impurities in the
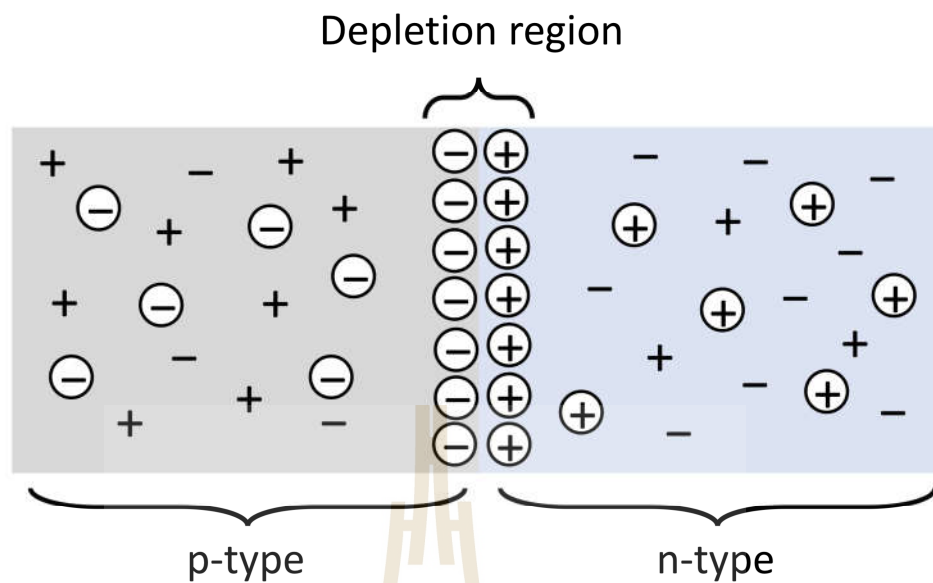
Figure 2.7 Forward bias PN-junction.

material), but the reduction in the width of the depletion region has resulted in a heavy majority flow across the junction. An electron of the n-type material now "sees" a reduced barrier at the junction due to the reduced depletion region and a strong attraction for the positive potential applied to the p-type material.
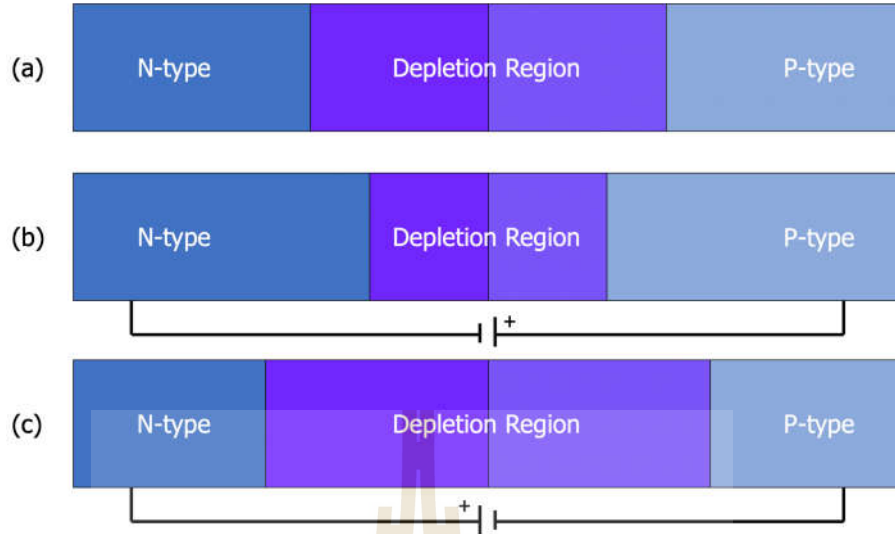
Figure 2.8 Representation of the relative depletion region for (a) no applied bias, (b) a forward bias and (c) a reverse bias semiconductor.

2.6 Monolithic Active Pixel Sensor (MAPS)

MAPS was chosen for the ALICE ITS upgrade. The design of ALPIDE sensors takes full advantage of the processing feature offered, in particular, the high integration density given by the availability of six metal layers and the small structure size as well as the deep p-well. The latter allows PMOS (P-type metal-oxide-semiconductor) transistors to be fabricated on a p-type epitaxial layer. By shielding their n-well from the epitaxial layer, it was not affected by charge collection, schematically as shown in Figure 2.9.

The particle detection principle of MAPS is through the interaction of a high energy particle and semiconductors sensor. While a particle is crossing the sensor, it generates electron-hole pairs along its path. Then these electrons diffuse until they reach the depletion region and drift toward the electrode where they are collected. The electrons will produce the signal in the electrode which is further processed by the electronic circuit (Greiner et al., 2011).
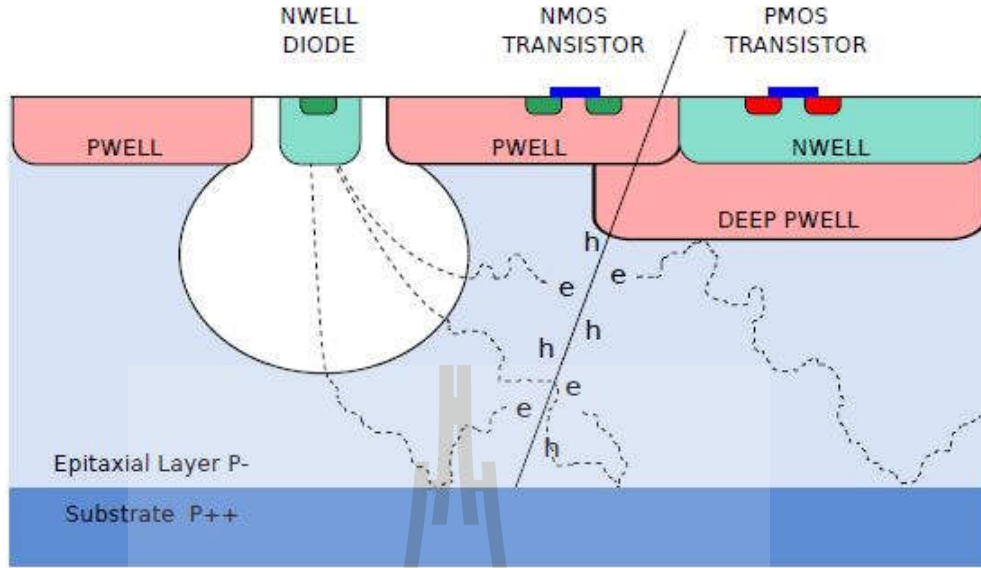
Figure 2.9 Schematic cross section of a MAPS pixel (Kofarago, 2015).

2.7 Development of MAPS for ALICE ITS upgrade

Since 2012, several prototype circuits have been developed and designed for the final ALPIDE chip. The first generation of the prototype is called Explorer. It modified the charge collection properties of the basic CMOS processor for improving the performance of the sensing node. The next generation in 2013, called pALPIDEss, was a prototype of the new low-power in-pixel intensification and separation front-end, which was the particular feature of ALPIDE. Since 2014, a full-scale sensor model, called pALPIDE-1, has been used to qualify the improvement in substantial scale gadgets. Consequent models, pALPIDE-2 and pALPIDE-3 proceed in including the rest of the elements, eminently the fast serial interface and the in-pixel various occasion memories (Mager, 2016).
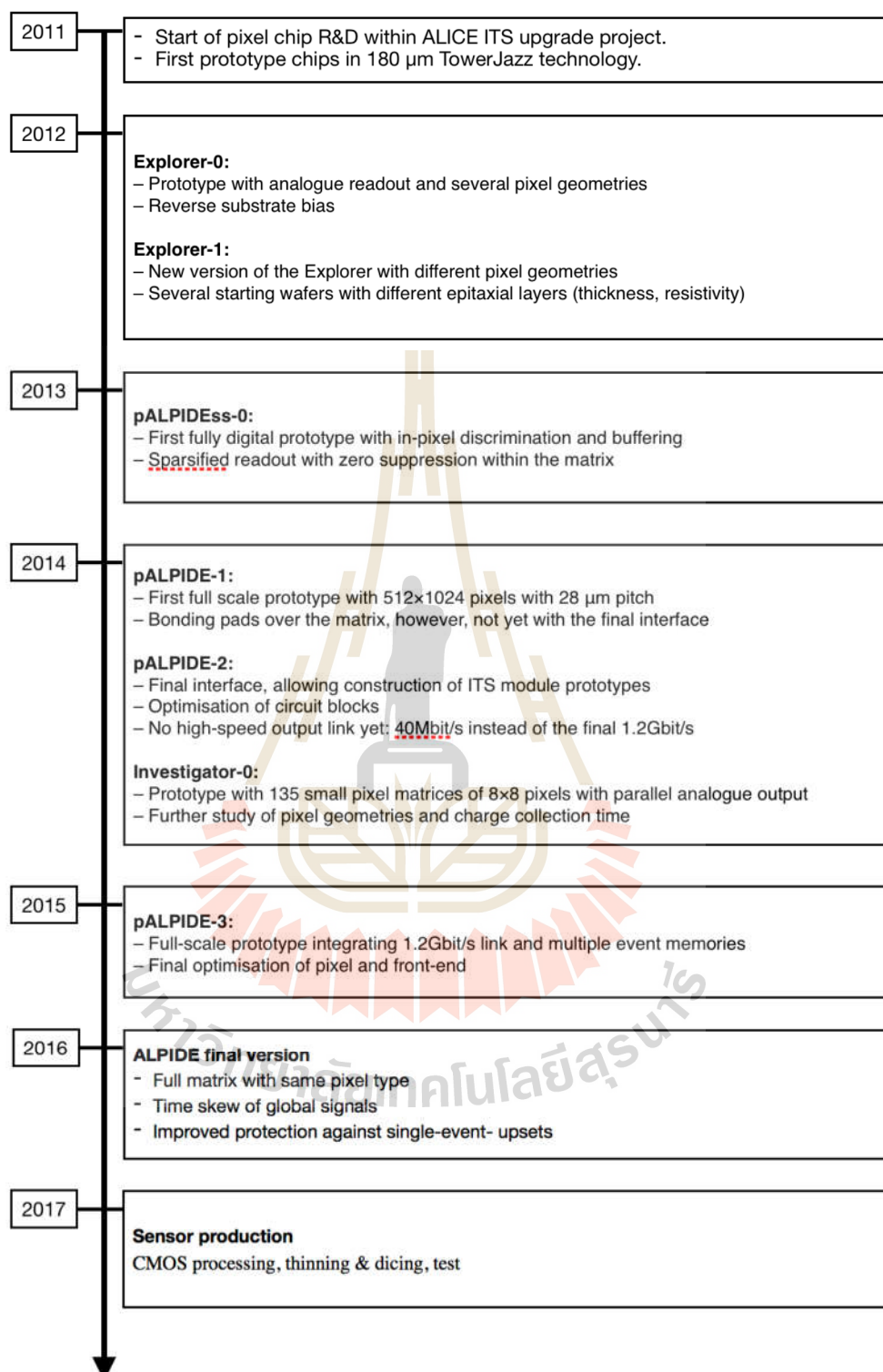
Figure 2.10 Timeline of the research and development for the new ITS pixel chip including the prototypes for the ALPIDE architecture.

CHAPTER III

COMMISSIONING OF THE SLRI BEAM

TEST FACILITY

3.1   SLRI accelerator complex

The Synchrotron Light Research Institute (SLRI) is the accelerator complex that provides synchrotron light. The synchrotron light is the electromagnetic wave radiated from charged particles such as electron moving at velocities close to the speed of light. Forced to change direction by actions of a magnetic field, such electrons then lose a certain amount of energy and discharge it in the form of electromagnetic waves called "synchrotron light."

In the production of the synchrotron light, the first step is to produce electrons by using a cathode of an electron gun. Then high positive voltage is applied to accelerate electron using a linear accelerator (LINAC). The purpose is to accelerate electrons to the desired energy (40 MeV). The electrons are then fed into the booster ring. In the third step, the particles in the synchrotron are forced to move in a circular pattern and accelerated until the electrons reach 1 GeV. Then the particles are transferred to the storage ring at the final stage. The storage ring increases the electron energy to reach up to 1.2 GeV. To produce synchrotron light, it requires magnetic field to change direction of electrons. The synchrotron light is provided to scientists for their various research. Figure 3.1 depicts a layout of the SPS injector and a location of the SLRI-BTF experimental area.

The SLRI accelerator complex includes:
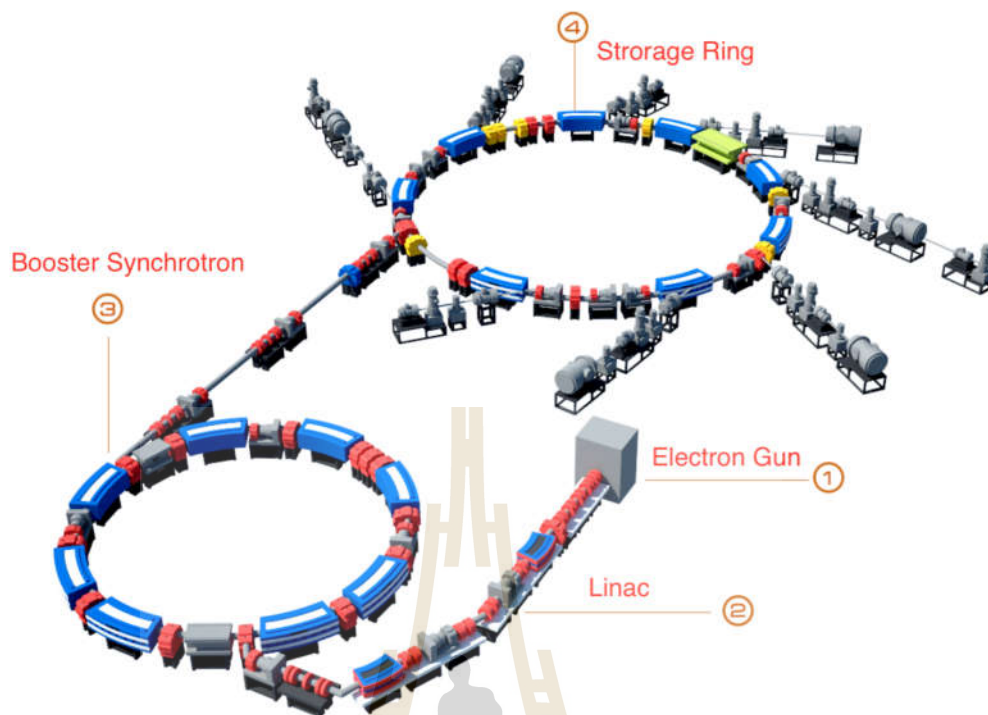
Figure 3.1 Schematic of the Synchrotron Light Research Institute(SLRI) (Synchrotron Light Research Institute (Public Organization), 2015).

1. Electron gun producing electrons by applying electricity to heat up the cathode until the electrons are released. Then high positive voltage is applied to pull the electrons into the linear accelerator.

2. Linear accelerator (LINAC) accelerating electron bunches by microwaves to attain 40 MeV. The electrons are then fed into the booster synchrotron.

3. The booster synchrotron that increases the electron energy in a circular motion by radio waves. To accelerate electrons to the desired energy by only a linear accelerator would require a length of several hundred-meters. However, scientists have come up with a circular accelerator which force the electrons to move in a circular pattern and accelerates until the electrons reach an energy level of 1 GeV in 0.6 seconds. The electrons are then

transferred into the storage ring at the final stage.

4. The storage ring increases the electron energy to 1.2 GeV. The ring consists of various types of magnets including dipole, quadrupole, and sextupole magnets which are used to force these high energy electrons to move in a vacuum tube. The energy, which is released in the form of electromagnetic waves, occurs in the bending magnet segment and is called "synchrotron light."

Table 3.1 Electron Beam Parameters at High-Energy Beam Transport Beam line (HBT). (Kittimanapun et al., 2016)

Particle	electron
Energy	1 GeV
Energy spread	-0.05%
Current	10 mA
Pulse duration	8.5 ns
Bunch length	0.5 ns
Repetition rate	0.5 Hz
Number of electron per burst	10^8

The electrons are injected into the storage ring twice daily in order to ensure sufficient intensity of synchrotron light produced. Due to the availability of the injector, SLRI has initiated the project that utilizes the high-energy electron beam by setting up a dedicated Beam Test Facility (BTF). SLRI-BTF aims to provide the controllable number of electrons, from a few to million electrons per bunch, with tunable energy by using the target chamber at the end of Low-energy Beam Transport beamline (LBT).

3.2   SLRI Beam Test Facility

The Synchrotron Light Research Institute Beam Test Facility (SLRI-BTF) is a part of the Synchrotron Light Research Institute (SLRI) accelerator complex. SLRI-BTF is the experimental station designed for testing detection efficiencies, spatial resolutions and the electron multiple scattering of the sensor. To complete the setup, essential requirement of this facility is the intensity of the electron beam, i.e., the number of electrons per burst which should be lower than ten particles. This can be accomplished by using the tungsten target with the wedge-shaped in the target chamber to reduce the intensity of electrons before entering synchrotron booster. Then the low-intensity electron beam with energy of 1 GeV will be transported to the Beam Test Facility (BTF) via the High-energy Beam Transport line (HBT) (Kittimanapun et al., 2016) and ready for the sensor characterization process.

The intentsity of the high energy electron beam is reduced by the target inside the chamber at the entrance of the synchrotron booster. Then, the high energy electron beam is extracted from synchrotron booster to HBT where a 4-degree bending magnet and two pairs of focusing and defocusing quadrupole (QF, QD) transfer the electron beam toward the SLRI-BTF experimental station. The electron beam position is controlled by using the magnet during transport from HBT to SLRI-BTF, as shown in Figure 3.2. A wedge-shape tungsten target has been employed and installed in the target chamber to decrease high-intensity electron beam at LBT. The location of a target chamber with the additional target to reduce high-intensity electron from the machine down to approximately 10 electrons per burst, is shown in Figure 3.5.

SLRI-BTF situates on the basement and shares an entrance with the SPS injector hall. Although SLRI-BTF is not running in the parasitic mode similar to
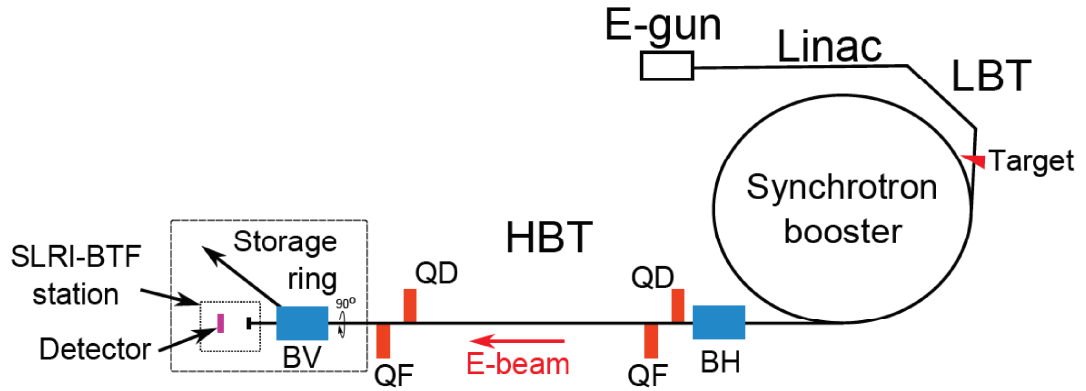
Figure 3.2 Layout of SLRI-BTF. Electrons from an electron gun are accelerated by a linac and transferred along the Low-energy Beam Transport beamline (LBT) to the synchrotron booster. High energy electrons are then extracted to the High-energy Beam Transport beam line (HBT) where a horizontal bending magnet (BH) and two pairs of focusing and defocusing quadrupole (QF, QD) direct the test beam to the SLRI-BTF experimental station located next to the vertical bending magnet (BV).

other beam test facilities, the beam transport parameters up to the synchrotron booster should be kept the same as ones used during the regular injection. With this constraint, the electron beam intensity has to be reduced online. It also provides the flexibility in adjusting the electron beam intensity changed due to fluctuation of electron beam current. Since the electron intensity is attenuated before entering the synchrotron booster, the desired energy of the test beam can be acquired by controlling acceleration time of the synchrotron booster. With resolution of 10 μm, the target thickness can be adjusted up to 6mm where the 40-MeV electron beam can be completely blocked. Slight tuning of quadrupole and steerer may be necessary to obtain desired beam profile at the SLRI-BTF experimental station. While SLRI-BTF is in operation, all components starting from the first vertical bending magnet (BV), which deflects the electron beam to

the storage ring, to the last component of HBT are turned off in order to avoid interference to the electron beam stored in the storage ring.

Electron beam parameters at HBT are listed in Table 3.1. Recently, the synchrotron booster has been upgraded and able to accelerate electrons up to 1.2 GeV. However, the repetition rate reduces to 1.3 Hz due to an increase of the ramping period of the bending magnet power supply.

Figure 3.3 Experimental area before construction the SLRI-BTF station, 3.5 m × 4.5 m.
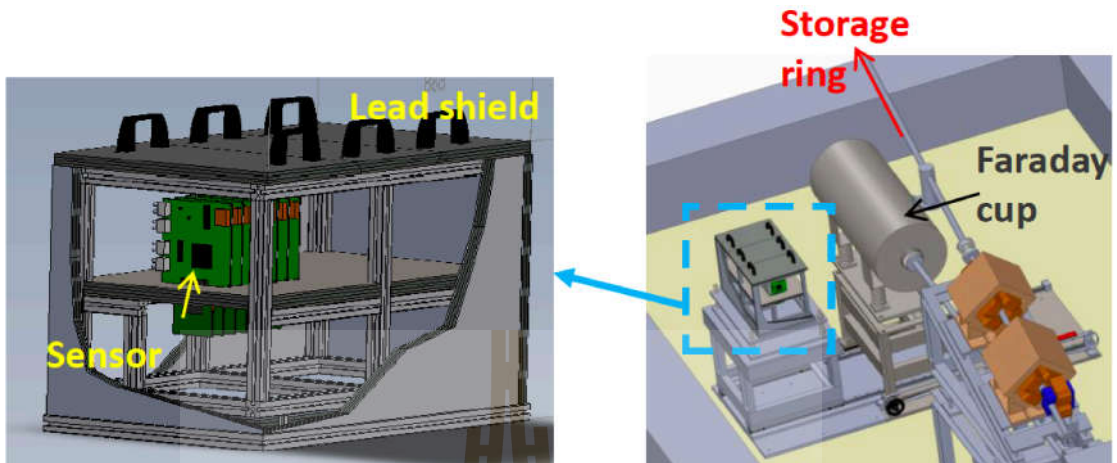
Figure 3.4 Pictures of the SLRI Beam Test Facility at the end of HBT line.
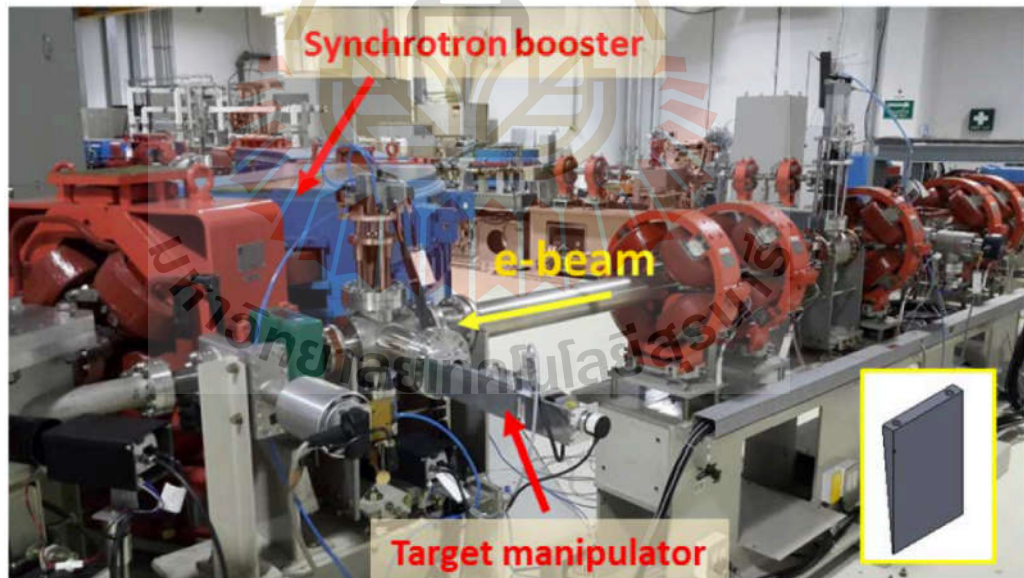
Figure 3.5 The photograph showing the LBT target chamber to reduce electron intensity before entering the synchrotron booster. An inset is the wedge-shape tungsten target.
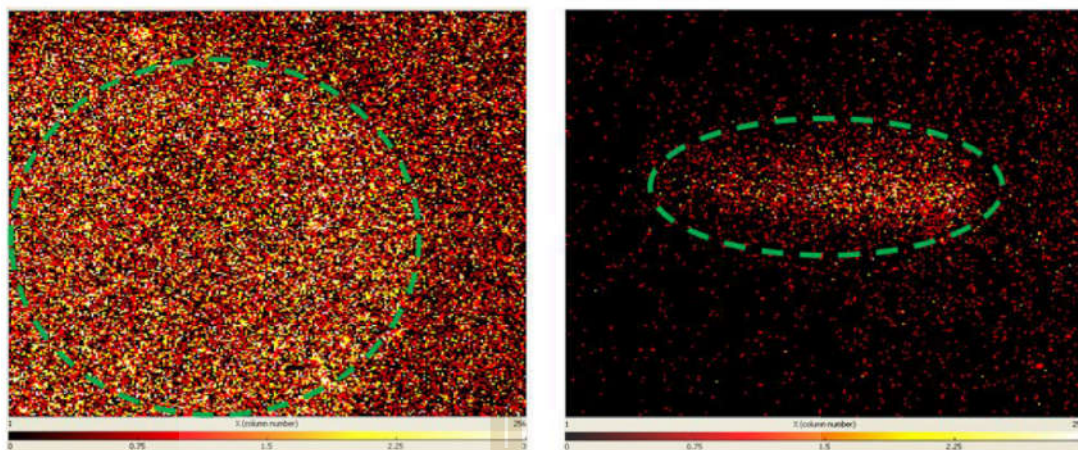
Figure 3.6 Distribution of high-energy electrons detected by the Timepix detector when the primary electron beam is attenuated by the HBT target (left) and the LBT target (right).

CHAPTER IV

TELESCOPE SETUP AT SLRI BTF

4.1 Principle of Beam Telescope

The detection efficiency represents the probability of a sensor to detect traversing particles. It is determined by two effects: first, the charge collected in the seed pixel (and the related distribution) which depends on the sensor geometry, the reverse substrate bias and the particle type, and energy; and second, the charge threshold. Consequently, lowering the threshold is beneficial for the detection efficiency, which is however limited by the involved increase of the fake-hit rate. Hence, a trade-off has to be found.

The detection efficiency is measured by using Minimum Ionizing Particles (MIPs) from a test beam facility and a beam telescope. The principle of beam telescope is schematically shown in Figure 4.1. A beam telescope is a particle tracking device, formed by several high-resolution position sensitive detectors, the so-called reference planes. The Device-Under-Test (DUT) is typically placed in the center of the telescope.

The results on the detection efficiencies presented in the following chapter have been obtained with a telescope of seven planes equipped with ALPIDE chips, where the central one plane were treated as DUT. Indeed, in this case the distinction between reference planes and DUT is only defined by the applied bias settings during the measurements. For the reference planes the settings are kept at fixed values, while for DUT they can be varied during the analysis (only the hit information from the reference planes is considered for track fitting). The anal-

ysis of the data has been performed using the EUTelescope framework, using a broken-line fit that considers multiple-scattering effects in the all planes.
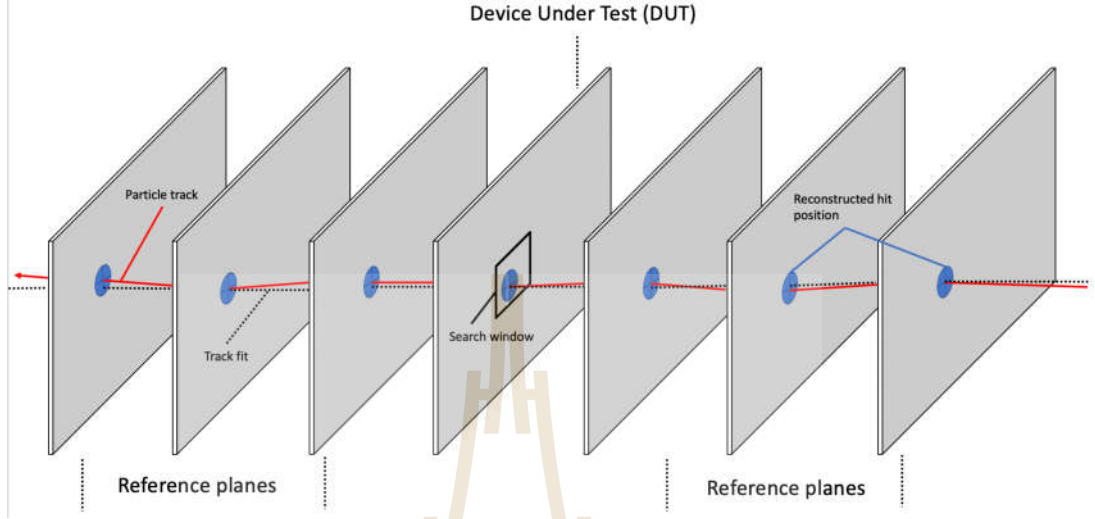
Figure 4.1 Principle of a beam telescope and the particle track fitting.

4.2 Design of Electron Beam Telescope

The ALPIDE prototype was mostly characterized by a soft X-ray source or MIPs from test beam facilities at CERN or DESY. The functionality and collection efficiency of the prototype were tested in the laboratory. Afterward, the ALPIDE prototype was investigated with the test beam for detection efficiency and spatial resolution measurements. The measurement uses several planes of the ALPIDE prototype perpendicularly aligned to the beam as a telescope as shown in Figure 4.2. The middle plane of the telescope is called DUT. The ALPIDE telescope was installed at SLRI-BTF for sensor characterization with high energy electrons of 1 GeV (see in Figure 4.2).

In this measurement, the telescope consists of seven planes of ALPIDE prototypes with 20 mm spacing. The ALPIDE sensor labeled as DUT is placed in the middle of an array of the reference planes. Once the beam passes through
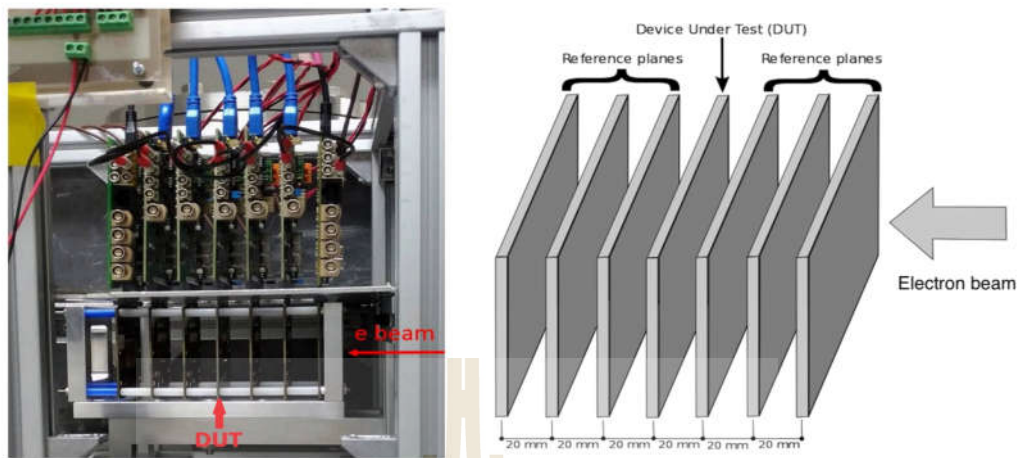
Figure 4.2 The ALPIDE telescope set up at SLRI-BTF. The middle plane is Device Under Test (DUT) and the others are reference planes.

sensor and telescope, the signal are detected and the track of the particle can be reconstructed. The analysis of this data is performed by the software developed by the ALICE ITS upgrade team based on EUTelescope framework. The flow chart and steps of the analysis are shown in Figure 4.3.
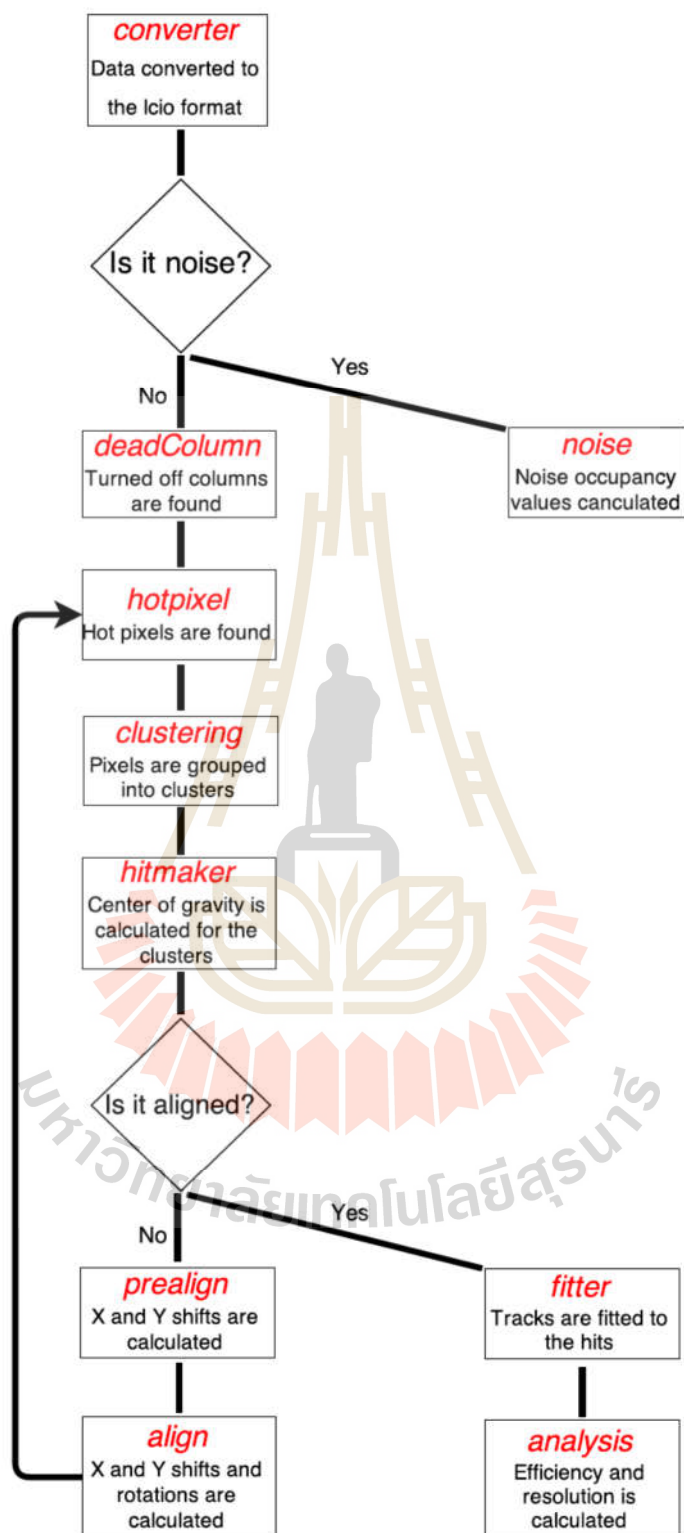
Figure 4.3 Flow chart of the analysis software base on the EUTelescope software frame work.

4.3 Sensor preparation

4.3.1 Laboratory test setup

A laboratory test is a test for a single sensor. The methods of characterization include functional test and a radiation hardness test.
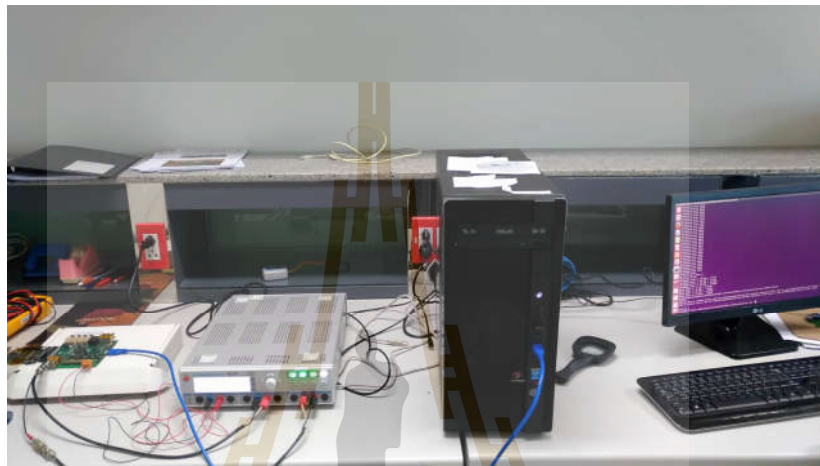
Figure 4.4 Laboratory Test Setup.

Figure 4.5 DAQ board (left) and pALPIDE sensor (right).

Trigger signal from circuit on sensor.

Analysis data from DAQ board.

Sensors → DAQ board → PC

Converter signal analog to digital.
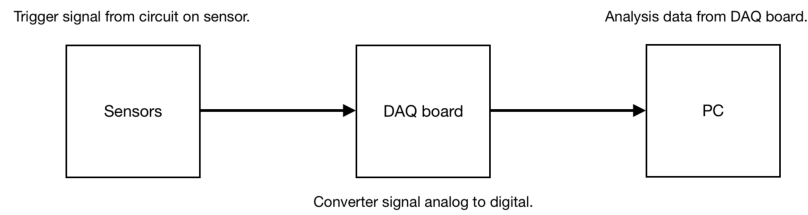
Figure 4.6 Diagram of laboratory test setup for ALIPIDE sensors.

4.3.2 Functional test

The functional test is a test to verify that the chip is fully functional. It is an incomplete characterization. In this test, we consider only three kinds of functional tests; a First-In First-Out (FIFO) test, an On-chip Digital to Analog Converter (DAC) test, and threshold scan.
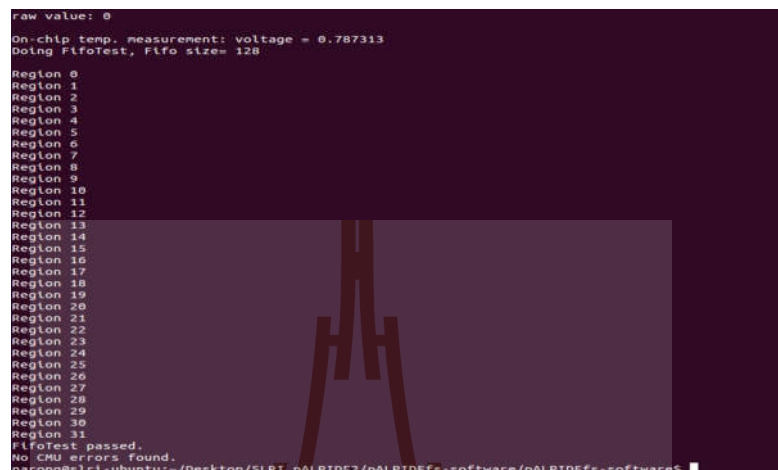
Figure 4.7 Functional test setup.

- The FIFO test examines the basic communication with the chip and also gives a first measurement of the current consumption before and after configuration. The FIFO test is a static random-access memory (SRAM) testing communication with the chip and checking both reading and writing of

SRAM. It also gives the first measurement of current consumption. The command is:

```
./runTest FIFO
```


Figure 4.8 Results of FIFO test. If it is successful, the screen will show a result similar to the above picture.

- The On-chip DAC test is a test for conversion of the binary inputs into analog voltage or current signal outputs. The output of the on-chip DACs can be related to monitoring pins of the pALPIDE chip. The command is:
  ```
  ./runTest SCANDACS
  ```

- The threshold scan is to test the detection analog performance of the pixels and trigger analog signals to sensors. The command is:

  ```
  ./runTest THRESHOLD 160 0 50
  ```

  where 160 is the number of mask states of the sensor, 0 and 50 is the range of the number of charge threshold.

To run the functional test software, we have to install the pALPIDE software, which is available in a git repository at CERN. Before testing, we have to download the firmware for processing chip on DAQ board.
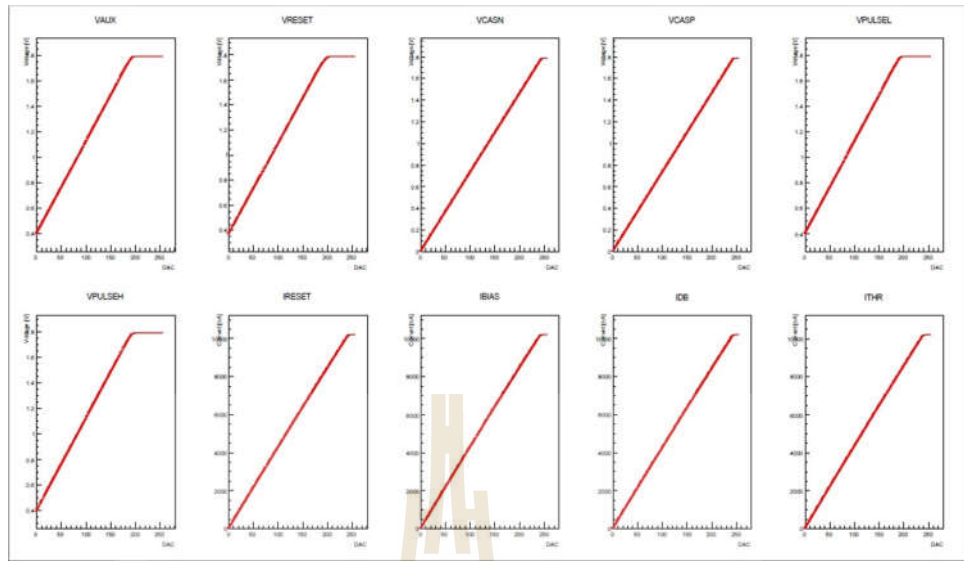
Figure 4.9 Results of the On-chip DAC test. The x-axis is amounts of DAC Digital to Analog Converter (DAC) from 0 to 255, and the y-axis is power consumption of DAC.
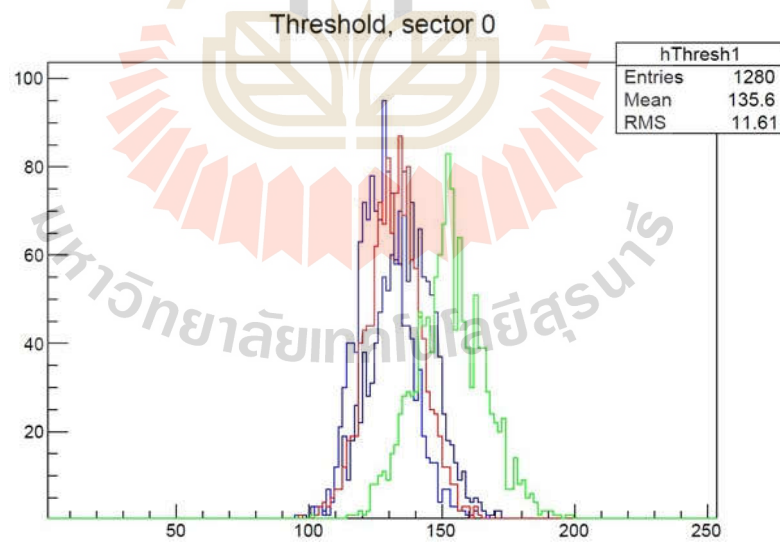
Figure 4.10 Results of threshold scan with 1% threshold scan. The x-axis is amounts of threshold (amounts of electron e^- from trigger signal) and the y-axis is the number of entries of each threshold. The different color in the graph is a different region in the sensor.

The firmware is available on the ITS upgrade Work Package 5 (WP5, https://twiki.cern.ch/twiki/bin/view/ALICE/ITS-WP5).

At the beginning, we have to check the DAQ board connectivity with computer by using the command:

```
./download_fx3 -t RAM -i SlaveFifoSync.img
```

If it is connected successfully, the computer screen will show the message "FX3 firmware programming to RAM completed".

The functional test has been successfully performed in the laboratory. All connection tests such as FIFO, DAQ scan are valid according to the design manual from the ALICE ITS upgrade project (ALICE Collaboration, 2014). All parameters of the circuits are also in good agreement with the design parameter and experiments carried out by the other ALICE collaborations, for example, the relation between the threshold distribution of the pixel chips and the front-end bias parameters ITHR and VCASN as shown in Figure 4.11. The threshold decreases' when VCASN increases, which is in good agreement with the results from the other groups.

Table 4.1 Table shown the results of functional test in the laboratory of pALPIDE-1, pALPIDE2 and ALPIDE sensors.

Chip id	Chip type	FIFO test	Scan DAC	Threshold scan
W9-17	pALPIDE-1	pass	pass	pass
W8-30	pALPIDE-1	pass	pass	pass
W14-9	pALPIDE-2	pass	pass	pass
W14-18	pALPIDE-2	pass	pass	pass
W14-12	pALPIDE-2	pass	pass	pass
W14-25	pALPIDE-2	pass	pass	pass
A4-W7	ALPIDE	pass	pass	pass
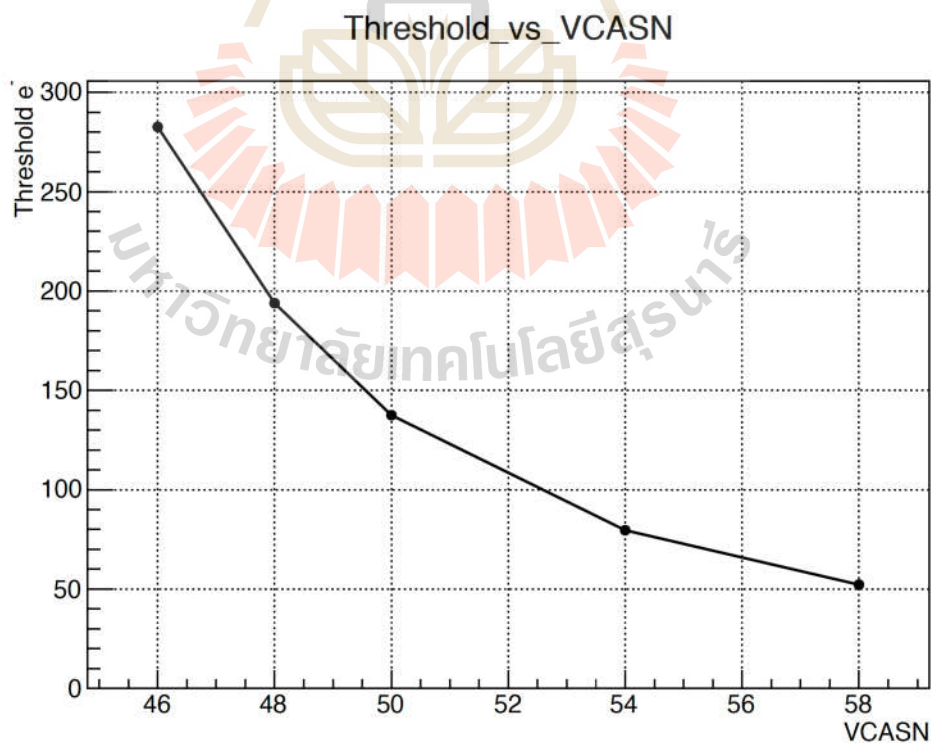
Figure 4.11 The relation between threshold distribution and VCASN.

4.4   Installation Telescope

4.4.1   Installation of the telescope at the BTF

The telescope was installed at SLRI-BTF for characterization of ALPIDE sensors, the middle plane DUT is the ALPIDE and two pALPIDE-1 and four pALPIDE-2 is the reference planes. The bias voltage for each plane are shown in the table 4.2
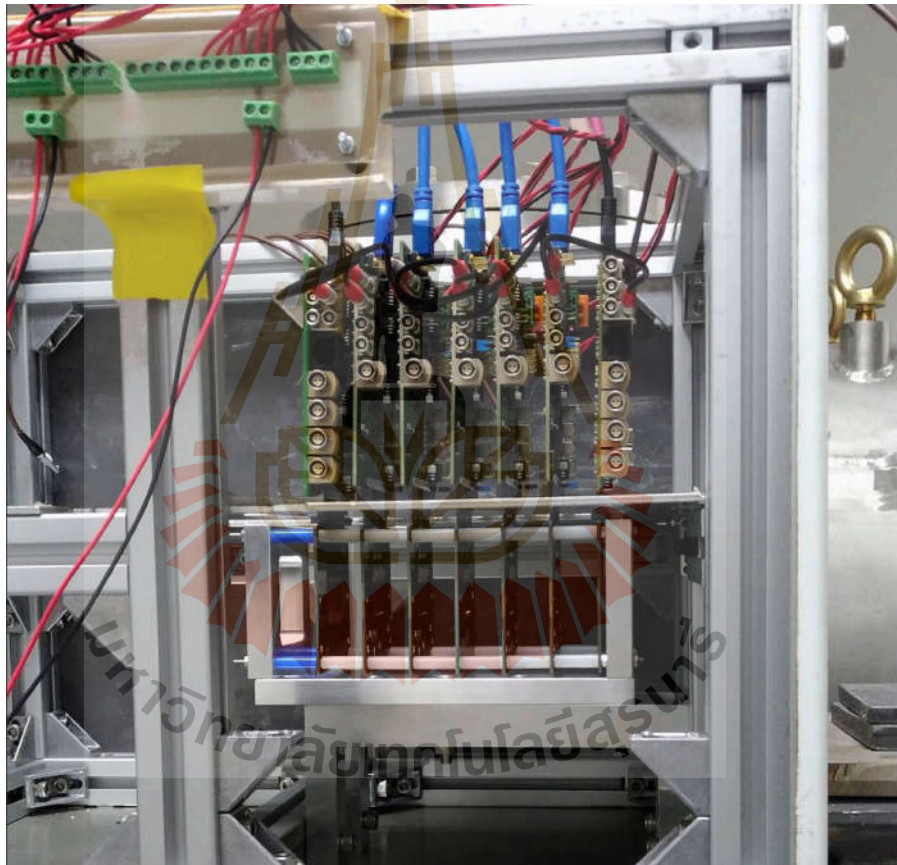
Figure 4.12 The photograph seven plane telescope setup at SLRI-BTF.

Table 4.2 Table shown the setting setup telescope at SLRI-BTF.

Plane number	Chip id	Chip type	Back bias voltage
1	W9-17	pALPIDE-1	0
2	W14-18	pALPIDE-2	-3
3	W14-9	pALPIDE-2	-3
4	A4-W7	ALPIDE	-3
5	W14-12	pALPIDE-2	-3
6	W14-25	pALPIDE-2	-3
7	W8-30	pALPIDE-1	0

4.4.2 Software

The software used to collect the data and shown in real-time during the test of sensors with the electron beam is called EUDAQ, written in C++, and designed to be modular and portable. The data files generated by the DAQ can be easily converted to the Linear Collider I/O (LCIO) format, allowing the data to be analysed with the EUTelescope.

The EUTelescope software is used to analyze the data collected from EU-DAQ by converting the data into the Linear Collider I/O (LCIO) format, then analyze and reconstruct the data taken with pixel beam Telescope.

CHAPTER V

COMMISSIONING RESULTS

5.1 First Test Beam Results

After the functional tests in the laboratory, we installed sensors in the telescope at SLRI-BTF for characterizing the sensors with 1 GeV electron beam. We wanted to observe raw hit map, correlation, the number of clusters, cluster size, hit vs plane and hit vs event for verifying that the sensors in the telescope can detect the electron beam from SLRI-BTF by the EUDAQ software.

Then, the raw data from the experiment were taken by the EUDAQ software and analyzed by the EUTelescope software for measuring detection efficiency of sensors in the telescope. The characteristics of the sensors from the EUDAQ will be given later in this chapter.

5.1.1 Raw hit map

The raw hit map graph shows the hitting position of the particle on sensors for each plane in the telescope. We observed the raw hit map by using EUDAQ software when the electron beam passed through sensors. The results of the raw hit map are used to verify that all sensors in the telescope can detect incoming electrons. Each blue dots in Figure 5.1 represents the hitting position of an electron on the sensor. The x-axis and y-axis in the graph are the number of pixels in the horizontal and vertical of the sensor, respectively.

If there is no blue dot seen in the graph, there may be some problems com-

ing from beam alignment, EUDAQ software configuration and sensor malfunction. In order to solve beam alignment problem, we have to adjust focusing and defocusing quadrupole magnet of SLRI-BTF for proper beam alignment. If it is a problem from EUDAQ software configuration, we have to modify DAC unit and the firmware of the sensors. But if the problem arises from sensor malfunction, we have to check the sensor in the laboratory test again.

In this test, we observed blue dots on every plane in the telescope, it meaned that all sensors in the telescope were working properly with good beam alignment and EUDAQ software configuration.
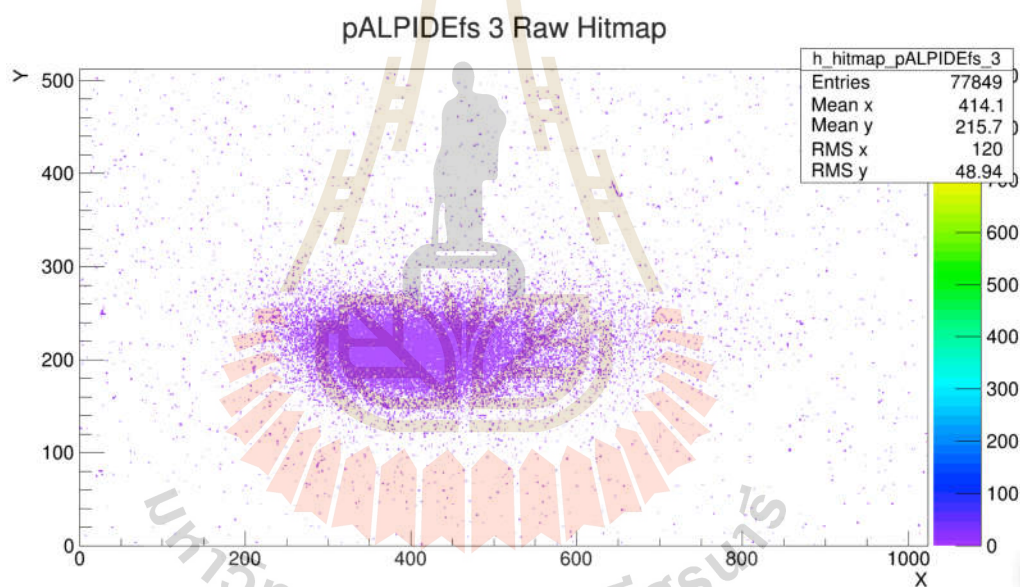
Figure 5.1 Raw hit map of the ALPIDE sensor. The blue dots seen in the figure represent the hit position of the 1 GeV electrons. Horizontal and vertical axes represents the sizes of the sensor.
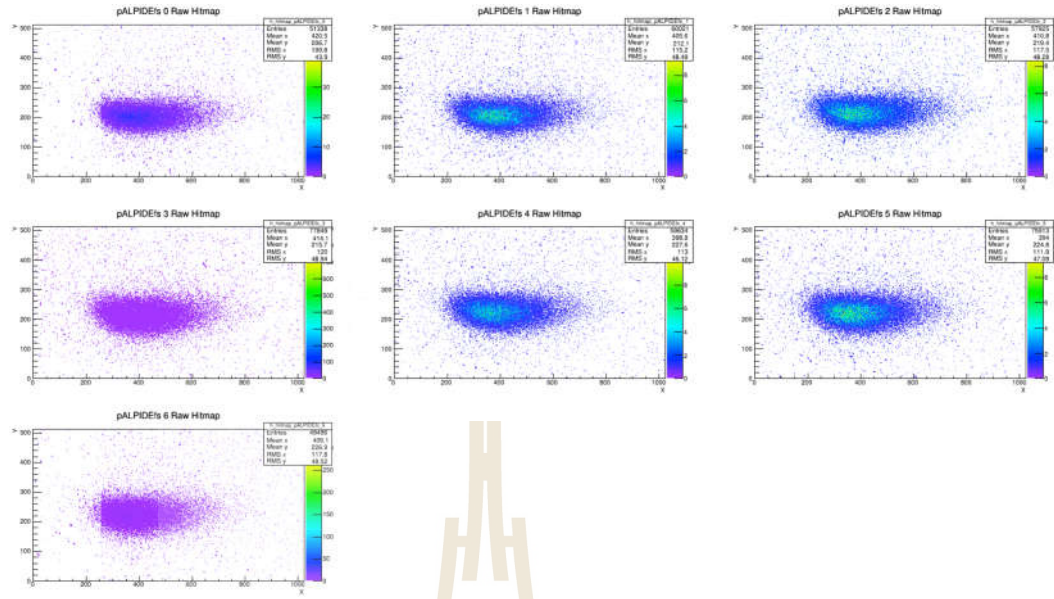
Figure 5.2 Raw hit map of the ALPIDE sensor seven planes in the telescope.

5.1.2 Correlation

Correlation plot is used to determine the position of the particle passing in the x and y axis between two different planes in the telescope. When we monitored the correlation during the electron beam test, the correlation plot should appear in the diagonal line due to particles traversing the same positions on nearby chips. It confirms that the electron beam passes through the telescope in a straight line.

The Figure 5.3 shows the correlation in x position between the third and the fourth planes. The horizontal axis is x position of the third plane, and the vertical axis is x position correlated to the fourth plane. The diagonal line in this graph shows the hit position of the electron beam at the same x position of the third plane and the fourth plane. The Figure 5.4 shows correlation of y position between third and fourth planes, the horizontal axis is y position of the third plane, and the vertical axis is y position correlated to the fourth plane. The diagonal line in this graph shows the hit position of the electron beam at the same y position of the third plane and the fourth plane.

In this graph, we observed the green cluster at the center. The green colour means the number of electrons hitting at the center are around 200 electrons or higher. The number of electrons can be seen in the colour bar on the right hand side of the graph. This occurs due to the spreading of electrons in the y direction, which is less than the spreading of electrons in the x direction. If there is no the diagonal line seen in this graph, we have to change the size of the beam spot by tuning the focusing and defocusing quadrupole magnet or adjusting the target manipulator of SLRI-BTF. In conclusion, the correlation graph that is used to verify the electron beam from SRI-BTF passing through the telescope is a straight line.
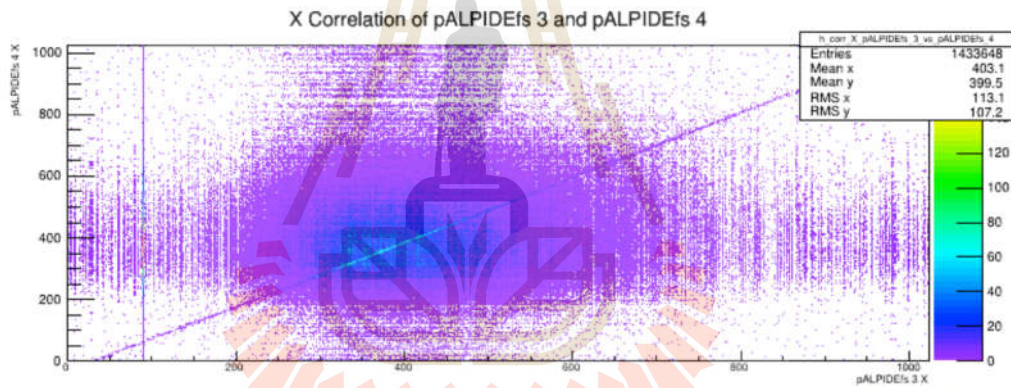
Figure 5.3 Correlations of the third plane with the fourth plane in the x position.
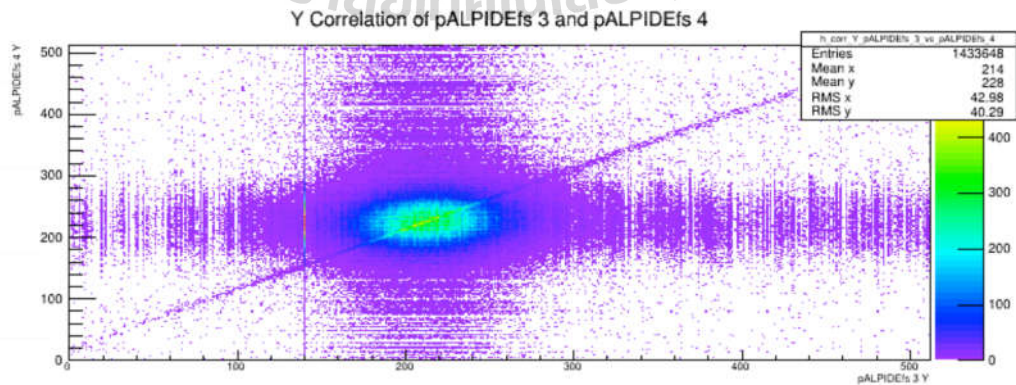
Figure 5.4 Correlations of the third plane with the fourth plane in the y position.

5.1.3 Cluster size

When a charged particle passes through the sensor, it generates more charges inside the sensor which can diffuse to one or more pixels nearby the particle passing point. Then the electronics signal is created.

The total signal will be shared by several pixels and the group of pixels which show a signal is called cluster size. Normally, the cluster size distribution depends on the settings of different parameters of the chip, the operating environment and the momentum of the measured particles.

But if we find a signal generated by only one pixel, not a cluster, it corresponds to the noise signal coming from bias voltage given to the sensors at threshold current is equal to 50 DAC unit in our test.

The preliminary results of cluster size of electrons from SLRI-BTF is shown in Figure 5.5. The horizontal axis is the cluster size with a unit in number of pixel and the vertical axis is the fraction of clusters. This set of clusters includes both the clusters originating from the crossing particle and also from the noise of the chip.
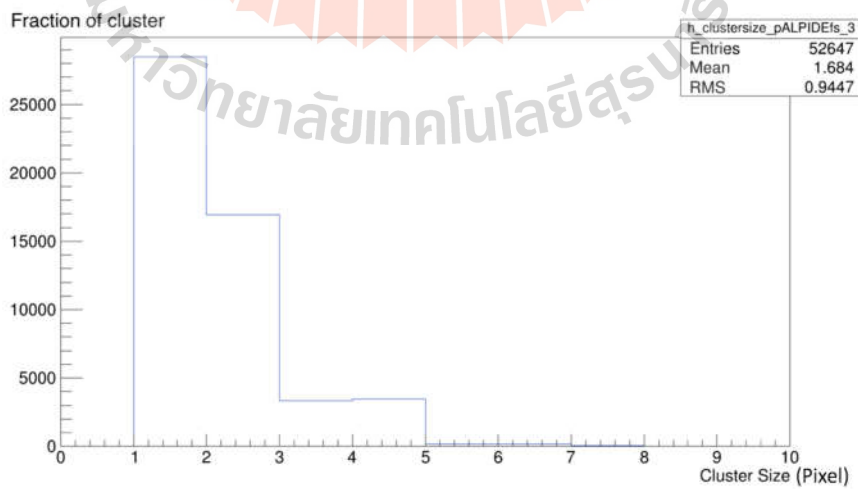
Figure 5.5 Cluster size of DUT, horizontal axis is the cluster size and vertical axis is the number of entries in each cluster size.

5.1.4 Number of clusters

One bunch of electrons generated at SLRI-BTF after using target manipulator consists of electron fewer than 10 electrons per bunch. Therefore when a bunch of electrons passes through the sensor in the telescope, it can generate a number of clusters. By looking at the number of clusters, we can get the information of number of electrons that hit on the sensors.

The figure 5.6 shows the histograms plots. The horizontal axis is the number of clusters, and the vertical axis is the amount of electron hit. The mean total of the hit number of electrons can be seen on the box in the right hand side of this graph. In this graph, we observed that the maximum of electron hit is around 5,000 when the number of clusters is equal to one.

In this result, we get the mean total of the hit number of electron on the sensor in the telescope which is around 3.67 electrons. These experimental results confirm that the inserted target manipulator is able to reduce the number of the electron of SLRI-BTF from 10^8 electrons per burst to around 10 electrons per burst.
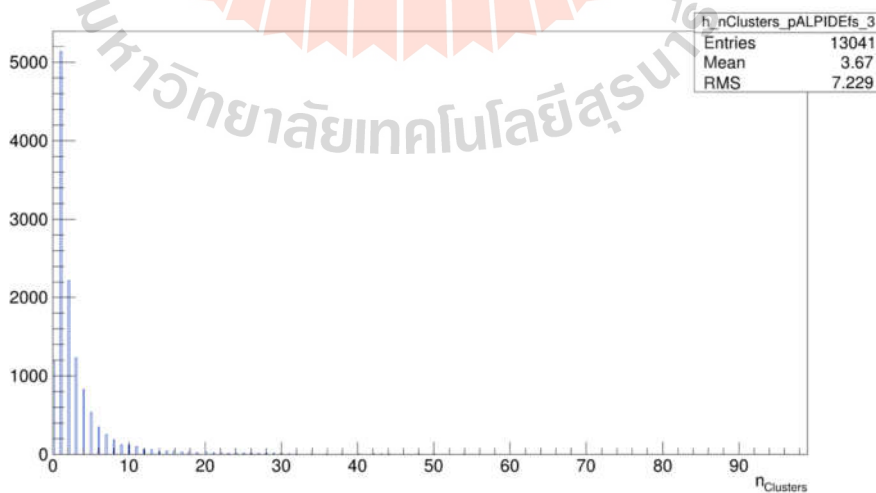
Figure 5.6 Detected number of clusters of DUT, x axis is the number of cluster and y axis is the number of entries in each number of cluster.

5.1.5   Hit vs plane

When a charged particle passes through on the sensors, the detection efficiency depends on the setting of different parameters of the sensor, the prototype of the sensor set in the telescope and the quality of sensors. In the telescope at SLRI-BTF, we installed the prototype of ALPIDE sensors, pALPIDE-1, pALPIDE-2 and ALPIDE.

The pALPIDE-1 is the first full scale prototype with 512 x 1024 pixels with 28 x 28 micrometer pitch, 4 sectors with different types of pixels, 1 register/pixel and no final interface. The pALPIDE-2 prototype was optimized the in-pixel and peripheral circuits and implemented final interface. But there is no high-speed output link (only a 40 Mb/s).

In the ALPIDE final version, there is one sector with full matrix of the same pixel type. It can operate up to 3 registers/pixel and equip with 1.2 Gbit/s data serial output. This sensor also comes with time skew of global signals and improved protection against single event upset. Overview and time line of sensor developments are already given in figure 2.10.

In our telescope at SLRI-BTF, there are 7 planes with 3 different type of sensors. We place pALPIDE-1 sensors in the first plane and the last plane, pALPIDE-2 sensors in the second, the third, the fifth and the sixth planes. In the fourth plane, which is in the middle plane of telescope, we put the ALPIDE sensor as the device under test (DUT).

Hits-vs-plane plots show the number of particles that hit sensor on each plane in the telescope. The horizontal axis is the sensor prototype each plane in the telescope and the vertical axis is the average number of particles hitting the sensors on each plane. The figure 5.7 shows the pALPIDE-1 sensors at the first and the last plane can detect the average number of hit between 3.8 to 4.2. The

pALPIDE-2 sensors at the second, the third and the fifth plane can detect the average number of hit between 4.4 to 4.6. Only the sixth plane can detect the average number of hit between 5.5 to 5.8. The ALPIDE sensor at the middle plane can detect the average number of hit between 6.6 to 7.

It can be seen that the ALPIDE sensor can detect the average number of hit better than pALPIDE-1 and pALPIDE-2 as expected. However, there is one of pALPIDE-2 in the sixth plane that is able to detect the average number of hit better than other pALPIDE-2. It may be affected by different quality of wafers used in the production of the pALPIDE-2 or different production lots at silicon chip foundry.
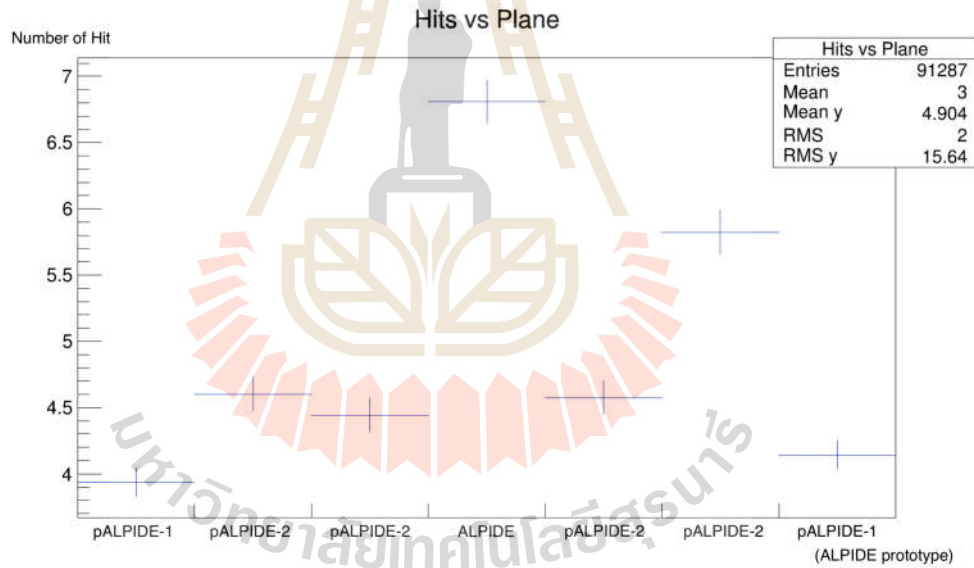
Figure 5.7 Hit each planes of the ALPIDE sensors of telescope. x axis is the number of plane in telescope and y axis is the number of particles hit on sensor.

5.1.6 Hit vs events

Hits-vs-event plots show the total number of particles that hit the sensors on the telescope per event. To obtain the total number of particle hits for each

event, we have to count the total number of particle hits on seven planes of sensors in the telescope. This means that, if we consider one event of a particle passing through the telescope in a strait line, the total number of particle hits will be seven hits. The horizontal axis is the number of events and the vertical axis is the total number of particle hit on the sensors in the telescope.

The figure 5.8 shows the total number of particle hitting the sensors in the telescope per event. To keep the average number of electrons around 10 electrons per burst, we use the target manipulator to reduce the number of particles hits in the range of 70 to 200 hits. However, during the measurement, we observe the fluctuation in the electron beam at the SLRI-BTF and this causes unusual increasing number of particle hits to 400, 600, 800 and 1,000 hit per event as seen in figure 5.8.

In this experiment, we found the maximum number of the particle hits on the telescope that make the read-out electronics circuit of the sensor to malfunction and cannot take the raw data, is around 1,500 hits. In order to solve the problem, we have to insert the target manipulator deeper for reducing the number of electrons hitting the sensors on the telescope.

After the data collection, the raw data has been analysed by the software based on EUTelescope framework described in the previous section. The important parameters such as detection efficiency and spatial resolution are then extracted. It is noted that these processes, especially data collection, are time consuming. The large number of hit particles (event) is required for good statistics. From our preliminary characterization, the detection efficiency which evaluates the number of tracked particle of DUT is as good as 99.6% was observed. This result is in good agreement with the CERN test beam experiment (Kofarago, M., 2016).
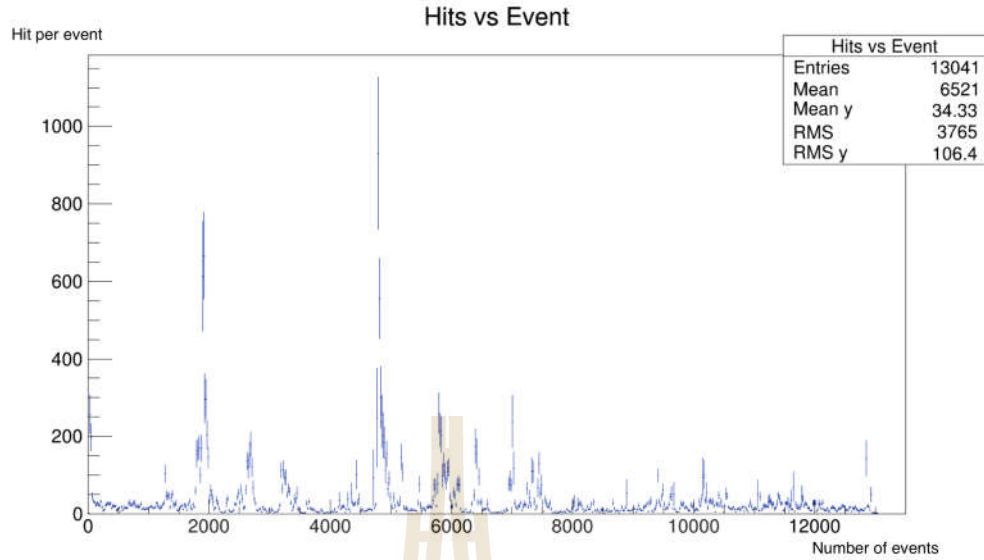
Figure 5.8 Hit per events of the ALPIDE sensor of telescope. X axis is the number of event and y axis is the number of particles each number of events.

5.1.7 Detection efficiency vs internal trigger measurement

We have to investigate the values of internal trigger delay of DAQ board matching with the main trigger of SLRI for measurement the detection efficiency of sensors. The detection efficiency is a measurement of the detection percentage of sensors from detected particles, which are emitted from the source. The internal trigger delay is an electronics circuit of sensors used to control the function of the DAC unit while the particle hit on the sensors and the main trigger of SLRI is the trigger signal of the electron beam produced from synchrotron booster that is delivered to the SLRI-BTF experiment station.

We measured detection efficiency of the sensor by varying the internal trigger delay value is 0, 35, 75, 115, 475, 600 and 800 on the DAQ board of DUT plane. The horizontal axis is the value of internal trigger delay of the DUT plane and the vertical axis is the value of detection efficiency of the DUT plane measured from the experiment. Figure 5.9 shows the detection efficiency of sensors depends

on the internal trigger delay.

In this results, when we increased internal trigger to be significantly larger than 475 the detection efficiency of a sensor will decrease. The detection efficiency of 99.6% was obtained at an internal trigger delay at 75.
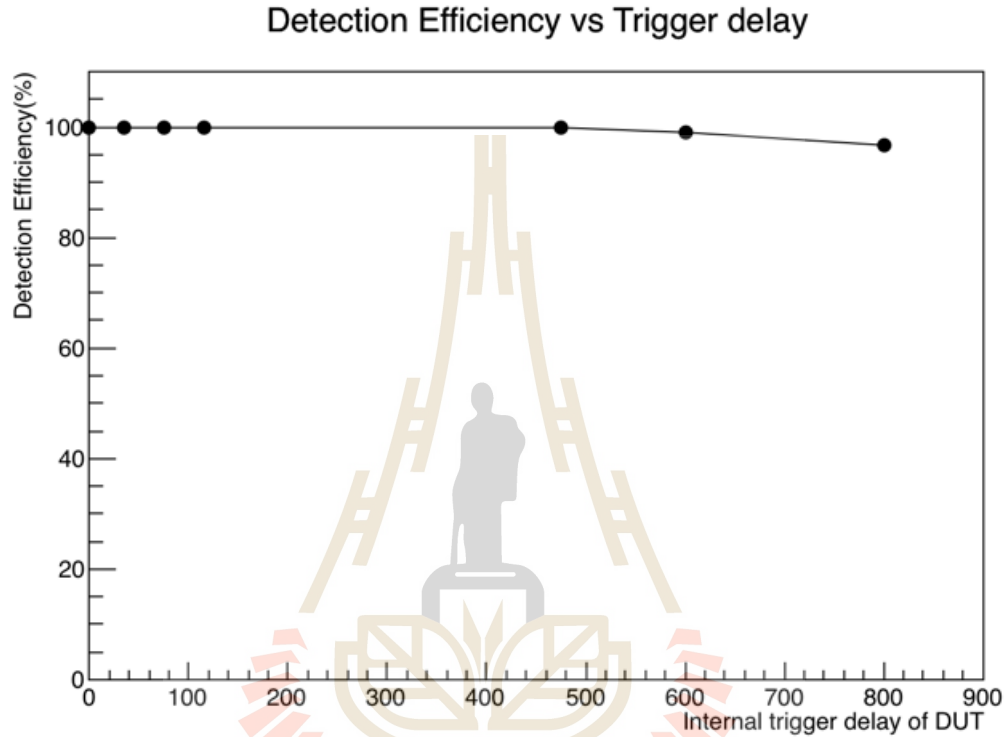
Figure 5.9 Detection efficiency corresponding to the trigger delay of the DAQ board, x-axis is the number of varying of trigger fo the DAQ board and y-axis is the detection efficiency of the ALPIDE sensors.

5.2 Commissioning of SLRI-BTF

SLRI-BTF has been prepared for installation of the telescope for testing of the ALPIDE sensors for the ALICE ITS upgrade project. Later, this station can be used to test other type of sensors.

In this work, we have to install telescope consisting of seven planes with

Figure 5.10 The SLRI Beam Test Facility at the end of HBT line before installation Telescope.

one ALPIDE as DUT, two pALPIDE-1 and four pALPIDE-2 as reference planes. In the future, we will install a new telescope consisting with all ALPIDE sensors for all seven planes to measure their detection efficiency.

We control the electron beam at SLRI-BTF by adjusting the target manipulator and the magnet of HBT, for finding the maximum number of electrons that the sensor can detect. The target manipulator is used to reduce the number of electrons before electron beam entering into the synchrotron booster ring. The magnet of HBT is used to change the shape and the position of the electron beam hitting on the sensor in the telescope.

The table 5.1 shows the number of hitting electrons measured from the SLRI-BTF on the sensors in the telescope. We observed the maximum number of electrons that the sensor can detect is 40 electrons per burst.

Table 5.1 Measurement result of the number of electron hitting on sensors.

Run number	Target	Time	Events	number of electron
289	61-63	6 Hr.	10550	20
317	59-65	6 Hr.	11024	10
320	64-67	6 Hr.	11306	5
352	63-66	6 Hr.	11032	30
359	62-65	6 Hr.	10361	35
417	63-67	6 Hr.	10798	40
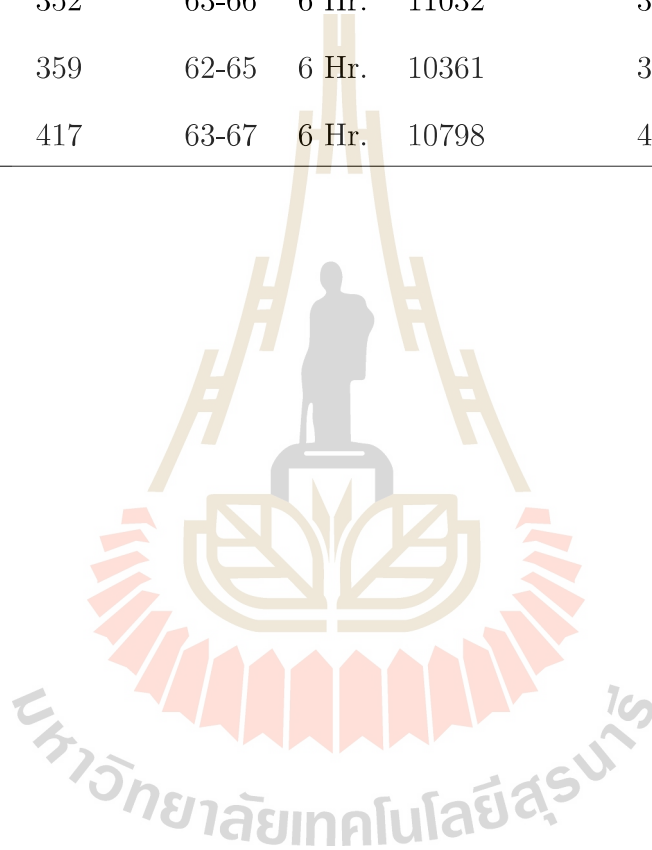
CHAPTER VI

CONCLUSION

In this work, we study the monolithic active pixel sensors called ALPIDE from ALICE, CERN. The prototype of ALPIDE sensors, pALPIDE-1, pALPIDE-2, and ALPIDEfs, have been tested in the laboratory for read-out electronics. After functional tests in the laboratory have been performed successfully, sensors have been installed on the telescope at SLRI-BTF for testing sensor with 1 GeV electron beam.

At SLRI-BTF we have installed software EUDAQ and EUTelescope. The EUDAQ is the software for taking the raw data and monitoring sensors on the telescope. Then we used EUTelescope to analyze data obtained from EUDAQ to get the detection efficiency of sensors. Comparing to DESY (5 GeV e^- in Hamburg, Germany), BTF (450 MeV e^- in Frascati, Italy), PAL (60 MeV e^- in Pohang, Korea), PS (6 GeV pion at CERN) and SPS (120 GeV pion at CERN), we use the 1 GeV electron beam to characterize sensors at SLRI-BTF.

At other test beam experiments, they use telescopes composed of the same type of sensors to measure the detection efficiency. But at the SLRI-BTF, our the telescope was made of 7 planes consisting of one ALPIDE as a DUT, two pALPIDE-1, four pALIDE-2 as reference planes. Therefore, we have to specifically optimize and configure software EUDAQ and EUTelescope for the telescope at the SLRI-BTF different from other test beam experiments.

The preliminary tested results show that the sensor well function according to the design specification wherewith the data taken from the measurement by the

EUDAQ software. Then the data has been analyzed by the EUTelescope software to measure the detection efficiency of the sensor. From our result, the detection efficiency of ALPIDE is 99.6%. Our result is in good agreement with the results from other test beam experiments at CERN and other institutes participating in the ALICE ITS upgrade project.

In the future, the electron beam generated from SLRI-BTF will be upgraded from 1 GeV to 1.2 GeV. We will characterize the ALPIDE sensors with the 1.2 GeV electron beam and measure the detection efficiency when the incident beam enters the DUT at a different angle.
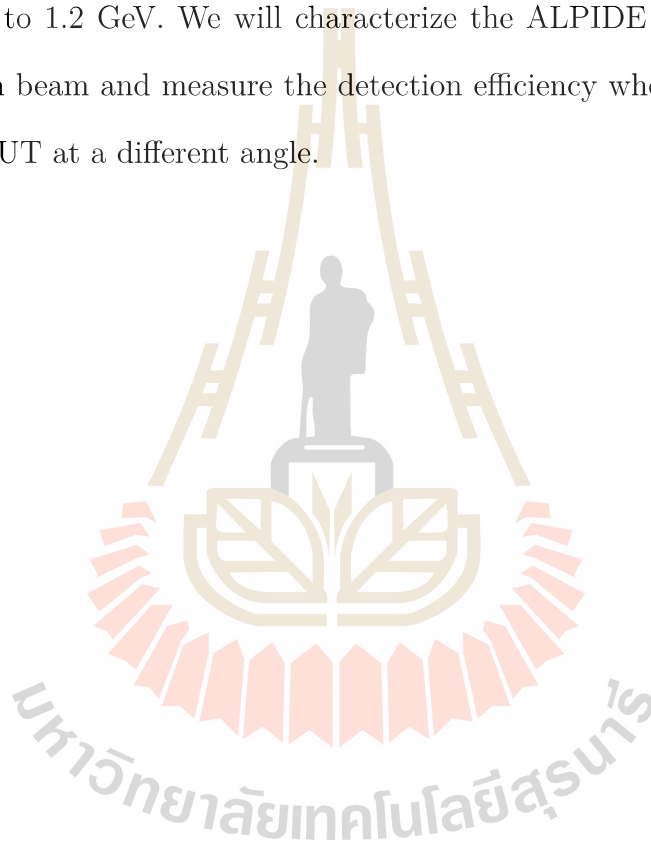
REFERENCES
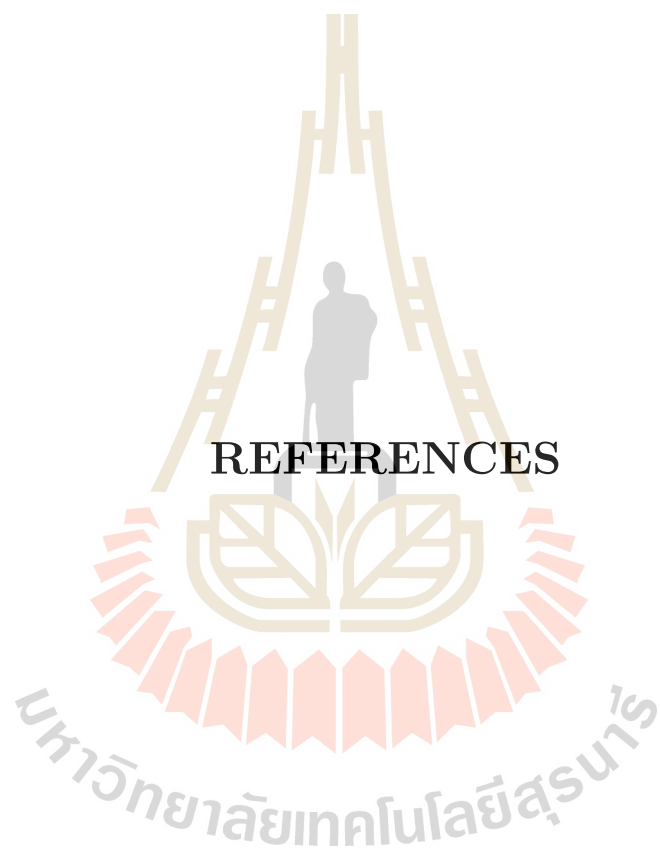
REFERENCES

Aamodt, K., Abrahantes Quintana, A., Achenbach, R., Acounis, S., Adamová, D., Adler, C., Aggarwal, M., and Agnese, F. e. a. (2008). The ALICE experiment at the CERN LHC. **Journal of Instrumentation.**

ALICE collaboration (2010). Alignment of the ALICE Inner Tracking System with cosmic-ray tracks. **Journal of Instrumentation.** 5(03): 03003.

ALICE collaboration (2012). Upgrade of the Inner Tracking System Conceptual Design Report. **Technical Report** CERN-LHCC LHCC-P-005.

ALICE Collaboration (2014). Technical Design Report for the Upgrade of the ALICE Inner Tracking System. **Journal of Physics G: Nuclear and Particle Physics.** 41.

Deutsches Elektronen Synchrotron (2018). EUDAQ framwork. **Retrieved from https://telescopes.desy.de/EUDAQ**.

Dorokhov, A., Bertolone, G., Baudot, J., Colledani, C., Claus, G., Degerli, Y., Masi, R. D., Deveaux, M., Dozière, G., Dulinski, W., Gélin, M., Goffe, M., Himmi, A., Hu-Guo, C., and Jaaskelainen, K. (2011). High resistivity cmos pixel sensors and their application to the star pxl detector. **Nuclear Instruments and Methods in Physics Research Section A: Accelerators, Spectrometers, Detectors and Associated Equipment.** 650(1): 174-177.

Greiner, L., Anderssen, E., Matis, H., Ritter, H., Schambach, J., Silber, J., Stezelberger, T., Sun, X., Szelezniak, M., Thomas, J., Videbaek, F., Vu, C.,

and Wieman, H. (2011). A maps based vertex detector for the star experiment at rhic. **Nuclear Instruments and Methods in Physics Research Section A: Accelerators, Spectrometers, Detectors and Associated Equipment.** 650(1): 68-72. International Workshop on Semiconductor Pixel Detectors for Particles and Imaging 2010.

Kittimanapun, K., Chanlek, N., Juntong, N., Cheedket, S., Klysubun, P., Krainara, S., Sittisard, K., and Supajeerapan, S. (2016). SLRI BEAM TEST FACILITY DEVELOPMENT PROJECT. **International Particle Accelerator Conference 2016.** page 2538.

Kittimanapun, K., Chanlek, N., Juntong, N., Cheedket, S., Klysubun, P., Krainara, S., Sittisard, K., and Supajeerapan, S. (2017). IMPROVEMENT OF ELECTRON INTENSITY REDUCTION SYSTEM AT SLRI BEAM TEST FACILITY. **International Particle Accelerator Conference 2017.** page 528.

Kofarago, M. (2015). Upgrade of the Inner Tracking System of ALICE. **Proceeding of science.** VERTEX2015: 009.

Kofarago, M. (2016). Test beam analysis with the EUTelescope framework. **Retrieved from https://twiki.cern.ch/twiki/bin/view/ALICE.**

Mager, M. (2016). ALPIDE, the Monolithic Active Pixel Sensor for the ALICE ITS upgrade. **Nuclear Instrumentsand Methods in Physics Research A.** 824: 434.

Nakamura, K. (2010). Review of particle physics. **Journal of Physics G: Nuclear and Particle Physics.** 37(7A): 075021.

Satz, H. (2011). The Quark-Gluon Plasma: A Short Introduction. **Nuclear Physics.** A862-863: 4-12.

Schambach, J., Anderssen, E., Contin, G., Greiner, L., Silber, J., Stezelberger, T., Sun, X., Szelezniak, M., Videbaek, F., Vu, C., Wieman, H., and Woodmansee, S. (2015). A maps based micro-vertex detector for the star experiment. **Physics Procedia.** 66: 514-519. The 23rd International Conference on the Application of Accelerators in Research and Industry - CAARI 2014.

Synchrotron Light Research Institute (Public Organization) (2015). What is Synchrotron Light. **Retrieved from http://www.slri.or.th**.

Yang, P., Aglieri, G., Cavicchioli, C., Chalmet, P., Chanlek, N., Collu, A., Gao, C., Hillemanns, H., Huang, G., Junique, A., Kofarago, M., Keil, M., Kugathasan, T., Kim, D., and Kim, J. (2015). Maps development for the alice its upgrade. **Journal of Instrumentation.** 10(03): C03030.

APPENDICES
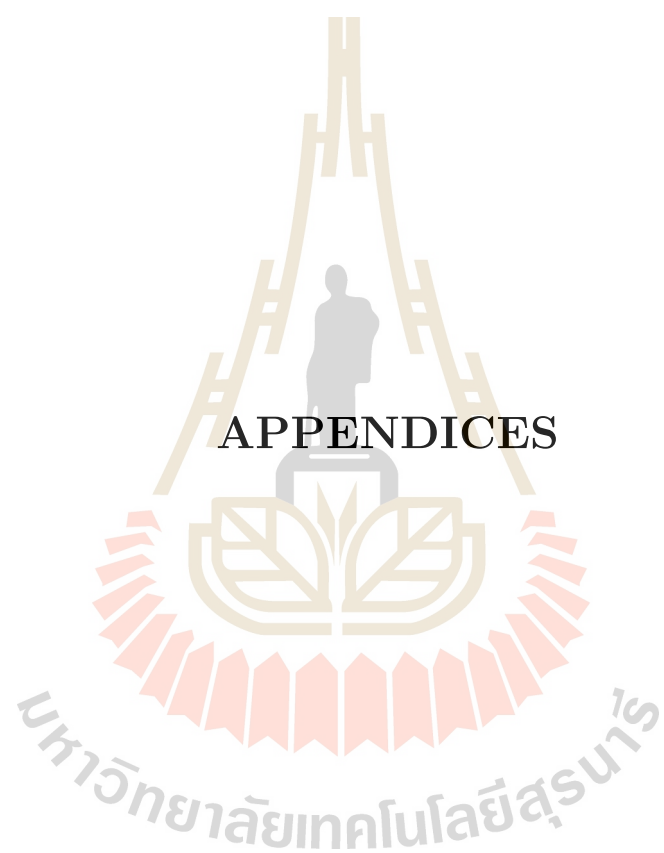
APPENDIX A

EUDAQ AND EUTELESCOPE SOFTWARE

INSTALLATION

The EUDAQ software is a data acquisition framework, written in C++, and designed to be modular and portable. The data files generated by the DAQ can easily be converted to the Linear Collider I/O (LCIO) format, allowing the data to be analysed with the EUTelescope) (Deutsches Elektronen Synchrotron, 2018).

To start the EUDAQ software execute

```
./STARTRUN
```

Four windows should open: the run control, the log window, the data collector and the pALPIDEfs producer. The run control window allows to power and configure the chips. Select the right configuration from the dropdown (palpidefs.conf) and click Config. Messages should appear in the log window and in the producer which report the successful initialization. Subsequently, one can start/stop runs with the corresponding buttons, to power down the cards, close the run control window. RAW data files are placed into the data directory.

To check the produced events one can use the online monitor. Although the name suggests that it can be used only online, it can be used with any RAW data file. It is started by

```
cd bin
./OnlineMon.exe -f FILENAME
```

By default the online monitor does not analyze each event. If this is desired,
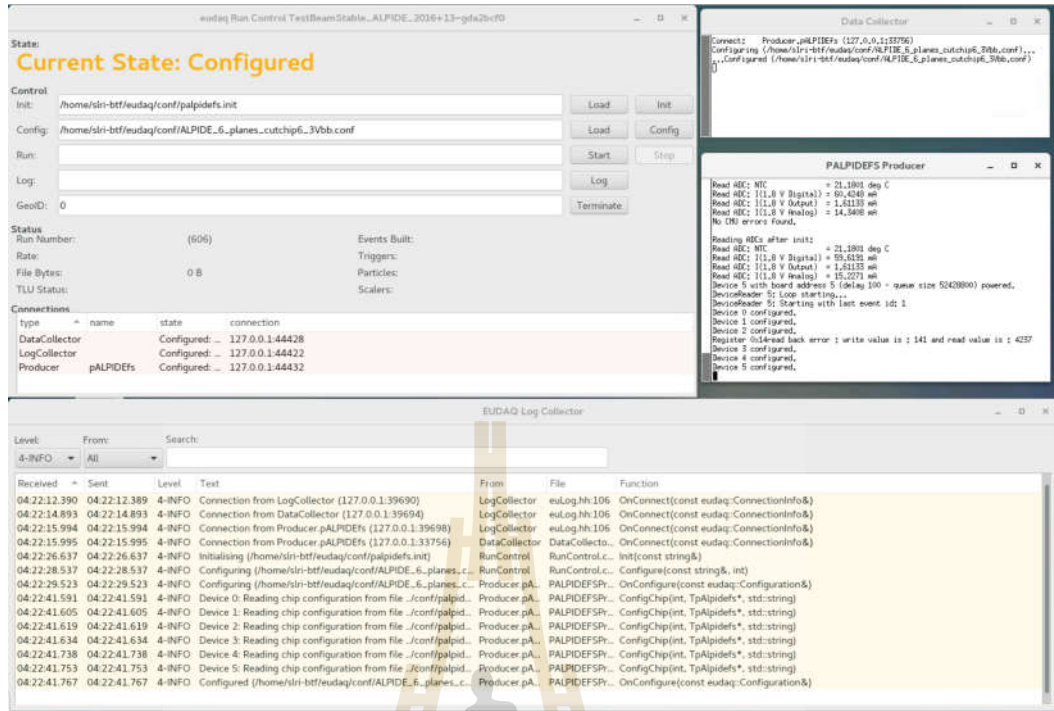
Figure A.1 The interface of EUDAQ software.

add the parameter -sc 0. The online monitor can also be started on a file which is of the ongoing run.

The EUTelescope framework is a group of Marlin processors to be used for analysis and reconstruction of data taken with pixel beam telescopes. It was implemented in the context of the EUDET project supported by the European Union in its 6th Framework Programme for the European Research Area and is embedded into the ILCsoft framework. The main goal of the EUTelescope software is to get from raw data to high level objects such as tracks crossing through the telescope. These tracks are used to characterize both the telescope itself and any other position sensitive detector (DUT = "device under test") that can be inserted into the telescope setup (Kofarago, M., 2016).

The EUTelescope software package was originally created as consistent data analysis chain for the EUDET telescopes. These telescopes consist of six planes

with high-resolution MIMOSA26 pixel sensors and are constructed to provide a full-featured infrastructure for DUT measurements. This includes the telescope with the sensors, cooling, and readout electronics as well as the Data Acquisition (DAQ) tool EUDAQ and the analysis software EUTelescope. The ILCsoft framework is being developed by the ILC community and unites several tools for data processing, originally intended for application in detector development efforts towards the International Linear Collider (ILC). The core elements of the framework are the Linear Collider I/O (LCIO) data model, the Geometry API for Reconstruction (GEAR) markup language and the event processor Modular Analysis & Reconstruction for the LINear collider (Marlin).

The implementation of EUTelescope into the ILCsoft framework and its modular structure have several advantages, such as the possibility to submit large analysis jobs for Grid computing and the possibility of a simple step-by-step analysis chain. Marlin allows the modular composition of analysis chains for various applications. Every task is implemented as an independent processor that is called by Marlin. The processors can expose parameters to the user which can be configured and loaded at runtime via so-called steering files in Extensible Markup Language (XML) format.

The main input of the full analysis chain is the LCIO output file produced by the DAQ system containing the pixel raw data. Along with that other data is also needed: for example calibration constants (pedestal and noise), eta distributions for each sensor and alignment constants. EUTelescope provides several processors for Marlin implementing algorithms necessary for a full track reconstruction and data analysis of beam test experiments. Most of the EUTelescope processors have been developed for the full-frame readout MIMOSA26 sensors and later adapted for zero-suppressed data. ILCsoft and EUTelescope installations are

available on the DESY Andrew File System (AFS).
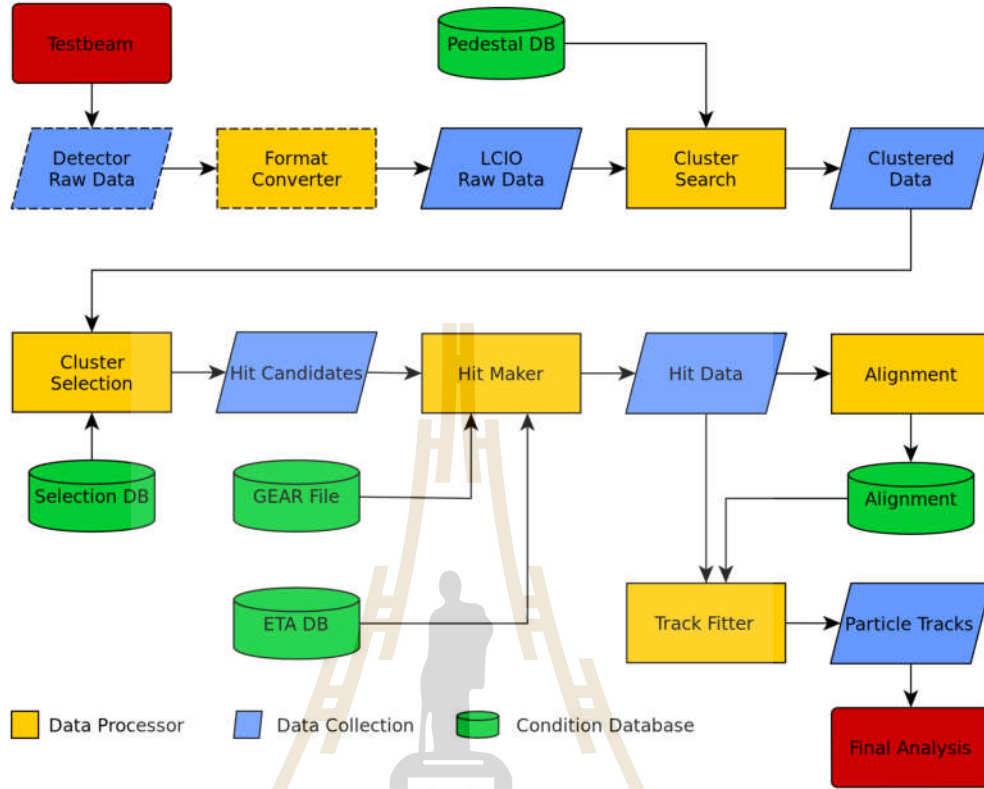
Figure A.2 flowchart of the EUTelescope framework.

There are two programs, EUDAQ and EUTelescope, for data collection and analysis of the beam test. In this section, we give some introduction on how to install and use these softwares.

- Installation and usage of EUDAQ.

    - Clone the repository by command:

        git clone https://github/eudaq/eudaq.git

        git checkout -b v1.7-dev origin/v1.7-dev

    - Go to the build directory and execute:

        cmake -DBUILD_onlinemon:BOOL=ON -DBUILD_palpidefs:BOOL=ON

        -DCMAKE_PALPIDEFS_DRIVER_INCLUDE:FILEPATH=/path/to/software/

Do not forget to change /path/to/software to the location of the pALPIDEfs software.

– To start data colletion by the EUDAQ, we execute `./STARTRUN` four windows should appear; run control, log window, data collector and pALPIDEfs producer windows. The run control window allows to configure the chips. To select the configure file, one can click at Config button. Messages should show through the log window and in the producer which reports the successful initialization. Subsequently, one can start/stop runs with the corresponding buttons. The events should be counted when we click the start button.

– We can check the produced events with the online monitor by going to the bin directory of EUDAQ software main directory and executing the command

`./OnlineMon.exe -f path/to/FILENAME (e.g.../OnlineMon.exe`
`-f ../data/raw000001)`.

- Installation and usage of EUTelescope on lxplus.

– Download install-eutelescope_lxplus.sh with the command:
`GIT_SSL_NO_VERIFY=true; git clone https://$(whoami)`
`@gitlab.cern.ch/alice-its-alpide-software/alice-its-upgrade`
`-eutelescope-installer.git` to the folder where you want to install. To start the installation we use the command

`./install-eutelescope_lxplus.sh`

– Go to the alice-its-alpide-test-beam-scripts directory which was created after successful installation, backup dataProcessing_ template.sh to another name. Edit the the new file in the first few lines to suit our

facility. Another file that we have to edit is the runlist_exmaple.csv which contains information about the energy of our beam, DUT number, chip ID, etc.

– Now, we can analyse raw data with the EUTelescope software by using the command:

```
./FILENAME.sh DEBUG number of the data
(e.g. ./dataProcessing_template.sh DEBUG 17)
```

APPENDIX B

SOFTWARE MODIFIED FOR DATA

ANALYSIS

Modified EUTelescope on lxplus for data analysis of the raw data from SLRI-BTF PC.

- Generate a new directory on your lxplus.

  `mkdir` slri-btf (just an example)

  install Eutelescope in your directory, the informed to install Eutelescope are available here:

  https://twiki.cern.ch/twiki/bin/view/ALICE/AnalysisInstallation

- Step to modified eudaq and palpidefs-software on lxplus.

  go to eudaq directory

  (/afs/cern.ch/work/n/nlaojamn/slri-btf-eutelescope/alice-its-upgrade-eutelescope-installer/v01-17-10/Eutelescope/master/external/eudaq/v1.7-dev)

  `git log -1` check your eudaq version git log <option>

  `git checkout 80b6fc8`

  recommend: you should be complied "source build_env.sh" in master directory (/afs/cern.ch/work/n/nlaojamn/slri-btf-eutelescope/alice-its-upgrade-eutelescope-installer/v01-17-10/Eutelescope/master)

- go to external directory, reinstall palpidefs-software.

(/afs/cern.ch/work/n/nlaojamn/slri-btf-eutelescope/alice-its-upgrade-
eutelescope-installer/v01-17-10/Eutelescope/master/external)
remove alice-its-alpide-software directory, reinstall palpidefs-software
by using this:

```
git clone https://nlaojamn@gitlab.cern.ch/alice-its-alpide
-software/alice-its-alpide-software.git
git checkout TestBeamStable_ALPIDE_2016
```

- go to pALPIDEfs-software directory, modified makefile same as below.
  **(/afs/cern.ch/work/n/nlaojamn/slri-btf-eutelescope/alice-its-
  upgrade-eutelescopeinstaller/ v01-17-10/Eutelescope
  /master/external/alice-its-alpide-software/pALPIDEfssoftware)**

```
CFLAGS= -pipe -fPIC -DVERSION = \"$(GIT_VERSION)\" -g
-std=c++0x -I /afs/cern.ch/work/n/nlaojamn/slri-btf-
eutelescope/alice-its-upgrade-eutelescopeinstaller/v01-17-10
/Eutelescope/master/external/libusb-1.0.3/ -I /afs/cern.ch/
work/n/nlaojamn/slri-btf-eutelescope/alice-its-upgrade
-eutelescopeinstaller/v01-17-10/Eutelescope/master/external
/tinyxml
LINKFLAGS=-lusb-1.0 -ltinyxml -L /afs/cern.ch/work/n/nlaojamn
/slri-btf-eutelescope/alice-itsupgrade-eutelescope-installer/
v01-17-10/Eutelescope/master/external/libusb-1.0.3/libusb-1.0
-L /afs/cern.ch/work/n/nlaojamn/slri-btf-eutelescope/
alice-its-upgrade-eutelescopeinstaller/v01-17-10/
Eutelescope/master/external/tinyxml
make clean
```

```
make

make lib
```

note: if you cannot do this step try to source build_env.sh in mater directory

- go to eudaq directory again, modified PALPIDEFSConverterPlugin.cc same as below.

(/afs/cern.ch/work/n/nlaojamn/slri-btf-eutelescope/alice-its-upgrade-eutelescopeinstaller/v01-17-10/Eutelescope/master/external/eudaq/v1.7-dev/main/lib/plugins)

- go to line 322

```
ifdef PALPIDEFS create DUT

switch(m_chip_type[i]) {

case 1:

m_dut[i] = new TpAlpidefs1((TTestSetup*)0x0, 0,

conf->GetChipConfig(), true);

m_daq_board[i] = new TDAQBoard(0x0, conf->GetBoardConfig());

m_daq_board[i]->SetFirmwareVersion(m_fw_version[i]);

break;

case 2:

m_dut[i] = new TpAlpidefs2((TTestSetup*)0x0, 0,

conf->GetChipConfig(), true);

m_daq_board[i] = new TDAQBoard(0x0, conf->GetBoardConfig());

m_daq_board[i] = new TDAQBoard2(0x0, conf->GetBoardConfig());

(add line)
```

```
m_daq_board[i]->SetFirmwareVersion(m_fw_version[i]);

break;
```

- go to line 697

```
PAYLOAD

{ if (m_chip_type[current_layer]<3) eventOK =

m_dut[current_layer]->DecodeEvent(&data[0]+payload_begin,

payload_length, &hits);

}

else if (m_chip_type[current_layer]==3) { // pALPIDE-3

TpAlpidefs3* p3 = dynamic_cast<TpAlpidefs3*>(m_dut[current

_layer]); if (p3) eventOK = p3->DecodeEvent(&data[0]+payload

_begin, payload_length, &hits, 0x0, 0x0, &statusBits);

}

else if (m_chip_type[current_layer]==4) { // ALPIDE

TpAlpidefs4* p4 = dynamic_cast<TpAlpidefs4*>(m_dut[current

_layer]); payload_begin+=24; (add line)

payload_length-=24; (add line)

if (p4) eventOK = p4->DecodeEvent(&data[0]+payload

_begin, payload_length, &hits, 0x0, &statusBits);

}

if (statusBits!=0) {

eventOK = false;

cout << "Status bits not 0x0 but " << statusBits << "!" <<

endl;

}
```

- go to build directory in eudaq folder

  (/afs/cern.ch/work/n/nlaojamn/slri-btf-eutelescope/alice-its-upgrade-eutelescopeinstaller/

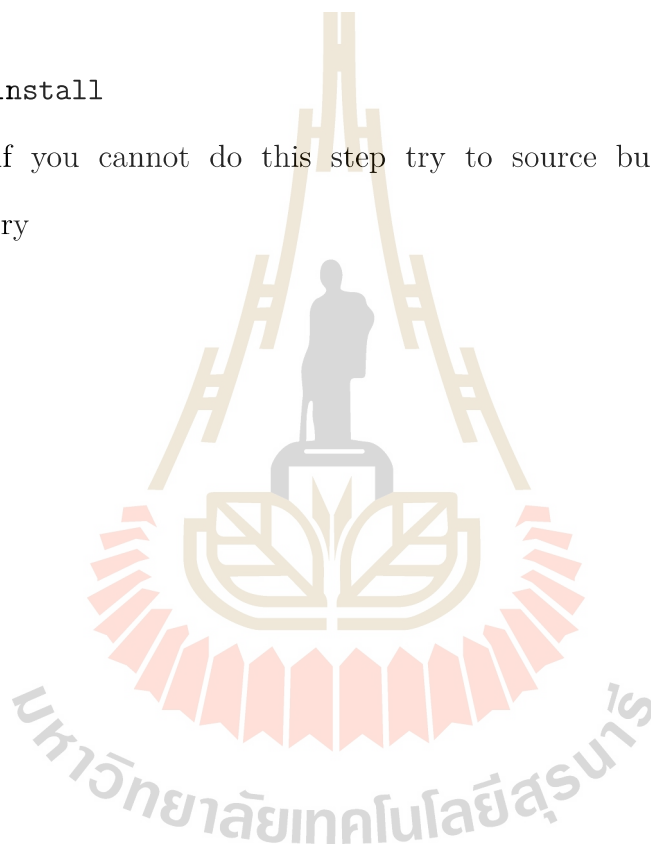 **v01-17-10/Eutelescope/master/external/eudaq/v1.7-dev/build)**

  cmake ../ -DCMAKE_PALPIDEFS_DRIVER_INCLUDE:FILEPATH=

  $(readlink -f ../../../alice-its-alpidesoftware/ pALPIDEfs-software/)

  ```
  make
  ```

  ```
  make install
  ```

  note: if you cannot do this step try to source build_env.sh in mater directory

CURRICULUM VITAE

NAME: Natthawut Laojamnongwong   **GENDER**: Male

NATIONALITY: Thai   **DATE OF BIRTH**: Nov 25, 1989

EDUCATIONS:

- B. Sc. Department of Applied Physics, Rajamangala University of Technology Isan, Thailand, 2012.

PUBLICATIONS

- Laojamnongwong, N. (2016). Preliminary Characterization of Monolithic Active Pixel Sensors with a 1 GeV Test Beam at SLRI Beam Test Facility. **The 7th International Graduate Research Conference (IGRC 7).** 211.